國 立 交 通 大 學

網路工程研究所

碩 士 論 文

應用於 MIMO-OFDM 時間同步之研究

The Study of Front-end Signaling and Timing

Synchronization in MIMO-OFDM systems

研 究 生：劉怡吟

指導教授：許騰尹 教授

中 華 民 國 九 十 六 年 六 月

應 用 於 MIMO-OFDM 時 間 同 步 之 研 究

The Study of Front-end Signaling and Timing Synchronization in MIMO-OFDM systems

研 究 生：劉怡吟　　　　　　Student：I-Yin Liu

指導教授：許騰尹　　　　　　Advisor：Terng-Yin Hsu

國 立 交 通 大 學
網 路 工 程 研 究 所
碩 士 論 文

A Thesis
Submitted to Institute of Network Engineering
College of Computer Science
National Chiao Tung University
in partial Fulfillment of the Requirements
for the Degree of
Master
in

Computer Science

June 2007

Hsinchu, Taiwan, Republic of China

中華民國九十六年六月

摘要

　　近幾年在無線技術發展下，新一代無線通訊系統中，正交分頻多工 (Orthogonal Frequency Division Multiplexing, OFDM)已經逐漸變成主流核心，在一個多路徑衰減的室內通道中，正交分頻多工被證明能有效的對抗由多路徑衰減所帶來的不理想因素。

　　本論文主要提出一個可以應用在 IEEE 所制定的無線區域網路標準 IEEE 802.11n 上之時間同步(Timing Synchronization)。其中 IEEE 802.11n 所使用的方式即為多輸入多輸出正交分頻多工 (Multi-Input-Multi-Output Orthogonal Frequency Division Multiplexing), MIMO-OFDM)。

　　本論文所提出之同步架構分為兩部份，一部分為封包同步 (Packet synchronization)，另一部份則為時間同步(Timing synchronization)。以上兩者主要皆為利用安置在每個封包內前端格式固定之 Preamble，在低訊號雜訊比和多路徑衰減的通道時可以快速，正確的達到同步。其中封包同步使用兩個 L-STS (Legacy Short Training Sequences)，而時間同步則只使用一個 L-STS。

Abstract

D UE to the explosive growth demand for wireless communications, the next-generation wireless communication systems are expected to provide ubiquitous, high-quality, high-speed, reliable, and spectrally-efficient. However, to achieve this objective, several technical challenges have to be overcome attempt to provide high-quality service in this dynamic environment [1].

Orthogonal frequency division multiplexing (OFDM), one of the multi-carrier modulation schemes, turns out to be a strong candidate for the future wideband wireless systems because of its high spectral efficiency and simplicity in equalization. However, OFDM also has its drawbacks. The notable issues of OFDM system are more sensitive to synchronization errors than single carrier system [2], [3]. Most OFDM synchronization methods have one or some of the following limitations or drawbacks: have a limited range of operation, address only one task, have a large estimation variance, lack robust sync detection capability, and require extra overheads [4].

In this work, we introduce a timing synchronization algorithm for 4*4 MIMO-OFDM systems. The synchronization scheme contains two partitions: One is packet synchronization, including packet detection and symbol boundary detection. By sharing resources, packet detection and symbol boundary detection detect simultaneously. It uses the first two Legacy Short Training Sequences (L-STS). The other is timing synchronization, particularly using only one L-STS (3_{rd} L-STS), both coarse and fine timing synchronization use a half L-STS.

Acknowledgement

Table of Contents

List of Figures

List of Tables

Symbol Description

AWGN   Additive White Gaussian Noise

BCB   Boundary Correlation Buffer

CFO   Carrier Frequency Offset

DAC   Digital To Analog

FEC   Forward Error Correction

FFT   Fast Fourier Ttransform

GI   Guard Interval

IFFT   Inverse Fast Fourier Transform

L-STS   Legacy Short Training Sequence

MIMO   Multi Input Multi Output

OFDM   Orthogonal Frequency Division Multiplexing

PPDU   PHY Protocol Data Unit

RMS   Root Mean Square

STBC   Space Time Block Code

$s(t)$ The transmitted signal

$y(t)$ The received signal

$w_k(t)$ Rayleigh-distributed tap gains

f_c Carrier frequency

f_m Maximum Doppler frequency shift

$S_j(k)$ The k_{th} transmitted signal from the j_{th} transmit antenna

$R_i(k)$ The k_{th} received time domain signal at the i_{th} receive antenna as $R_i(k)$

N_{ij} The additive white Gaussian noise between the j_{th} transmit antenna and the i_{th} receive antenna

u_i The decision variable on the i_{th} receive antenna

P_L FFT size

Pc GI size
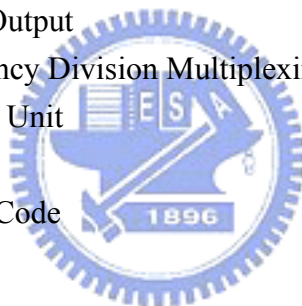
$Q(k)$ L x B matrix

$P_{i,L}(k)$ Correlation power

ϕ Phase error

Chapter 1

Introduction

D UE to the explosive growth demand for wireless communications, the next-generation wireless communication systems are expected to provide ubiquitous, high-quality, high-speed, reliable, and spectrally-efficient. However, to achieve this objective, several technical challenges have to be overcome attempt to provide high-quality service in this dynamic environment [1].

Orthogonal frequency division multiplexing (OFDM), one of the multi-carrier modulation schemes, turns out to be a strong candidate for the future wideband wireless systems because of its high spectral efficiency and simplicity in equalization. However, OFDM also has its drawbacks. The notable issues of OFDM system are more sensitive to synchronization errors than single carrier system [2], [3]. Most OFDM synchronization methods have one or some of the following limitations or drawbacks: have a limited range of operation, address only one task, have a large estimation variance, lack robust sync detection capability, and require extra overheads [4].

In this work, we introduce a timing synchronization algorithm for 4*4 MIMO-OFDM systems. The synchronization scheme contains two partitions: One is packet synchronization, including packet detection and symbol boundary detection. By sharing resources, packet detection and symbol boundary detection detect simultaneously. It uses the first two Legacy Short Training Sequences (L-STS). The other is timing synchronization, particularly using only one L-STS (3_{rd} L-STS), both coarse and fine timing synchronization use a half L-STS.

This thesis is organized as follows. In Chapter 2, a brief introduction of MIMO-OFDM system is given, including IEEE 802.11n physical layer transmitter, receiver and wireless channel model. In Chapter 3, the proposed synchronization

algorithm for 4*4 MIMO-OFDM systems is presented. The simulation results are shown in Chapter 4. Proposed hardware architectures are presented in Chapter 5. Finally, this thesis is concluded in Chapter 6 and reference is in the last part of this thesis.
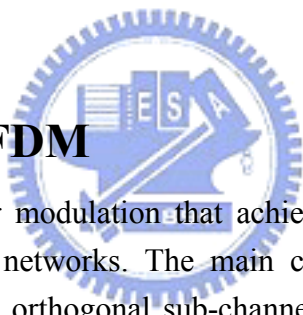
Chapter 2

System Platform

IN this chapter, the basic of OFDM is introduced. Three main blocks of wireless communication: transmitter, receiver, and channel model are described as follows.

2.1 The Basic of OFDM

OFDM is a multi-carrier modulation that achieves high data rate and combat multipath fading in wireless networks. The main concept of OFDM is to divide available channel into several orthogonal sub-channels. All of the sub-channels are transmitted simultaneously, thus achieve a high spectral efficiency. Furthermore, sub-carriers have orthogonal property and carried individual data. Their spectrum overlaps are zero. It is easy to use FFT and IFFT to implementation OFDM. However, OFDM has its drawbacks. The significant one is sensitivity to synchronization errors. The synchronization errors come from two sources. One is the local oscillator frequency difference between transmitter and receiver, and the other is the Doppler spread due to the relative motion between the transmitter and the receiver [5]. In addition, timing synchronization may affect the performance of channel estimation [6].

2.2 IEEE 802.11n Physical Layer Specification

2.2.1 Transmitter

The IEEE 802.11n is know as multi-input-multi-output OFDM system

(MIMO-OFDM), operating in both 2*2 and 4*4 antennas to transmit and receive data and support higher coding rate up to 5/6. Figure 2-1 shows transmitter data path. First use FEC encoder to encodes the source data. FEC encoder supports 1/2、2/3、3/4、5/6 four kind coding rates. Then the bit stream is parsed into spatial streams, according to the number of transmit antennas. The interleaver provides a form of diversity to guard against localized corruption or bursts of errors. And then, the QAM mapping is used to modulate the bit stream. It supports BPSK, QPSK, 16 QAM, 64 QAM, 64 QAM or 256 QAM. After QAM mapping, the constellation points pass through Alamouti Space Time Block Code (STBC) encoder. The STBC encoder spreads the constellation points of each spatial stream to any other spatial streams. IFFT is used to transfer signal from frequency domain to time domain. In 20MHz, there are 64 frequency entries for each IFFT, or 64 sub-carriers in each OFDM symbol, 52 of them are data carriers, 4 of them are pilot carriers, other are null carriers. After Insert Guard Interval (GI), the signal is transmitted by RF.
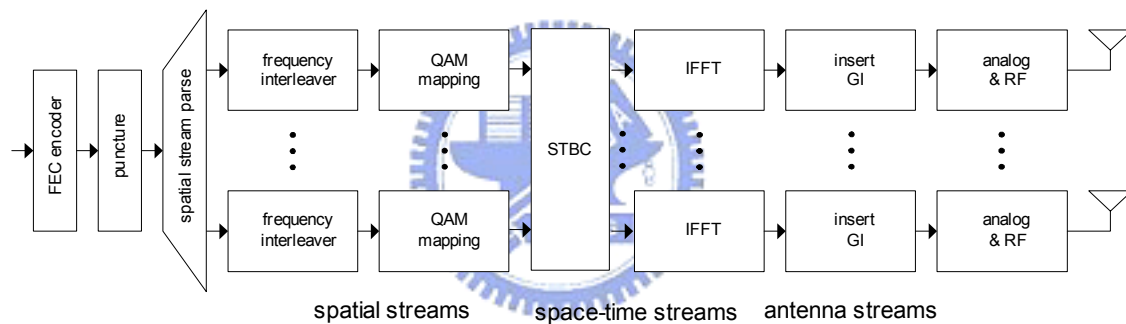
Figure 2-1: IEEE 802.11n transmitter data path [7]

2.2.2 Receiver

Figure 2-2 shows receiver data path. The signal is received form the RF. Sync is used for synchronization, including to find when exactly the packet start, the OFDM symbol boundary and the best sample phase. After a packet is presented, FFT is used to transfer received signal from time domain to frequency domain. Channel effect will be estimated and compensated by Equalizer. IQ mismatch is also taken under consideration. After all estimation and compensation, Alamouti STBC decoder is used to combine four bit streams into original. Then the bit streams are de-map, de-interleave and merge to single data stream. Finally, it is decoded by FEC which includes de-puncturing, Viterbi decoder and de-scrambler.
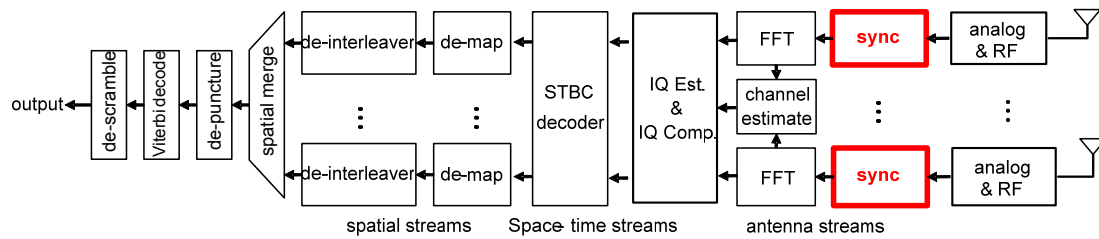
Figure 2-2: IEEE 802.11n receiver data path

2.2.3 Basic MIMO PPDU Format

A PHY protocol data unit (PPDU) is defined to provide interoperability. Figure 2-3 shows the PPDU format for the basic MIMO mode. Each packet contains a header (ex. L-STF, L-LTF, …) for detection, channel estimation and synchronization purposes. First part is the L-STF which can be used for signal detection, AGC stabilization, diversity, coarse acquisition …etc. The L-STF is formed by the repetition of ten L-STS of 16 samples each; these samples have correlation properties. In this thesis, correlation techniques will be applicable for packet detection, symbol boundary detection, and timing synchronization. A detail data structure of L-STF is shown as Figure 2-4.
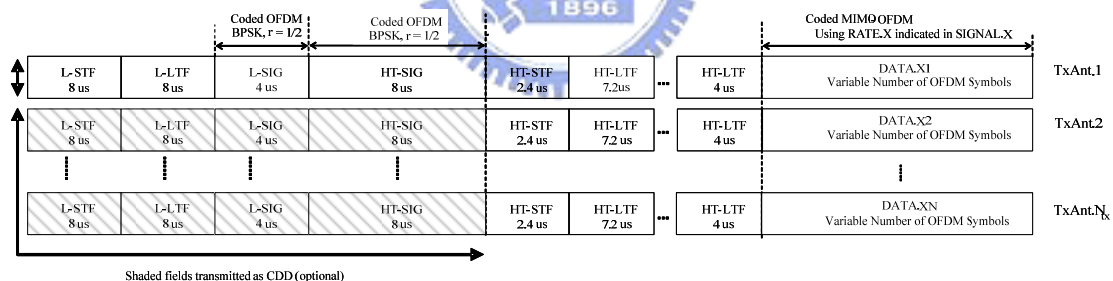
Figure 2-3: PPDU Format for NTX antennas [7]
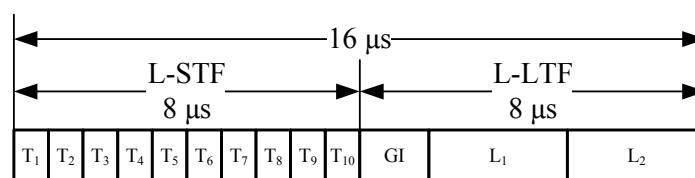
Figure 2-4: OFDM training structure include of L-STF and L-LTF [7]

2.3 Channel Model

There are many imperfect effects during transmitted signals through channel, such as Additive White Gaussian Noise (AWGN), carrier frequency offset (CFO), multipath, and so on. The block diagram of channel model is shown in Figure 2-5.
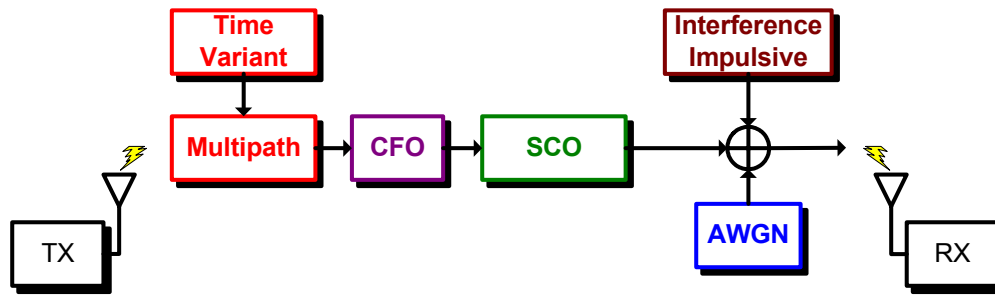
Figure 2-5: Block diagram of channel model

2.3.1 Additive White Gaussian Noise

Wideband Gaussian noise comes from many natural sources, such as the thermal vibrations of atoms in antennas, "black body" radiation from the earth and other warm objects, and from celestial sources such as the sun. The AWGN channel is a good model for many satellite and deep space communication links. On the other hand, it is not a good model for most terrestrial links because of multipath, terrain blocking, interference, etc. The signal distorted by AWGN can be derived as

$$r(t) = s(t) + n(t) \tag{2.1}$$

where $r(t)$ is received signal,

$s(t)$ is transmitted signal,

$n(t)$ is AWGN.

2.3.2 Multipath

Because there are obstacles and reflectors in the wireless propagation channel, the transmitted signal arrivals at the receiver from various directions over a multiplicity of paths. Such a phenomenon is called multipath. It is an unpredictable set of reflections and/or direct waves each with its own degree of attenuation and delay. Multipath is usually described by two sorts:

A. Line-of-sight (LOS): the direct connection between transmitter and receiver.

B. Non-line-of-sight (NLOS): the path arriving after reflection from reflectors.
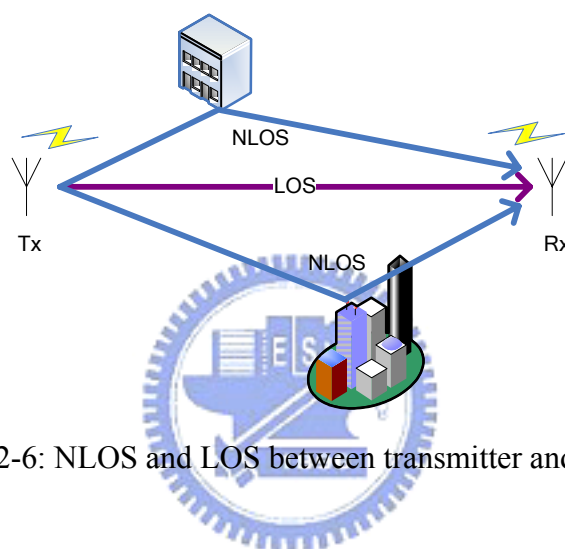
Figure 2-6: NLOS and LOS between transmitter and receiver

Multipath will cause amplitude and phase fluctuations, and time delay in the received signals. When the waves of multipath signals are out of phase, reduction of the signal strength at the receiver can occur. One such type of reduction is called the multipath fading; the phenomenon is known as "Rayleigh fading" or "fast fading." Besides, multiple reflections of the transmitted signal may arrive at the receiver at different times; this can result in inter symbol interference (ISI) that the receiver cannot sort out. This time dispersion of the channel is called multipath delay spread which is an important parameter to access the performance capabilities of wireless systems. A common measure of multipath delay spread is the root mean square (RMS) delay spread as shown in Table 2-1. For a reliable communication without using adaptive equalization or other anti-multipath techniques, the transmitted data rate should be much smaller than the inverse of the RMS delay spread (called coherence bandwidth). A representation of Rayleigh fading and a measured received power-delay profile are shown in Figure 2-7.

Table 2-1: TGn multipath channel types[15]

Model	LOS/NLOS	RMS delay spread (ns)	# of taps
A	NLOS	0	1
B	LOS	15	2
C	LOS/NLOS	30	5
D	NLOS	50	8
E	NLOS	100	15
F	NLOS	150	22
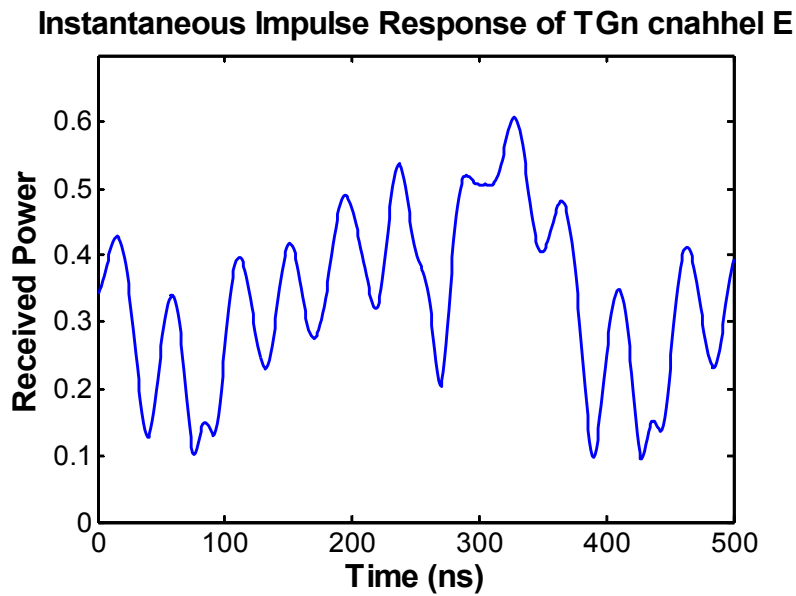
Figure 2-7: Instantaneous impulse responses

2.3.3 Time Variant Jakes' Model

Time-variant channel effect can be modeled as a FIR filter with time-variant tap gains. For Jakes' model, the variance of each tap gain obeys Rayleigh distribution. Figure 2-8 shows an n-tap FIR filter with Rayleigh-distributed tap gains, and the corresponded velocity is 120km/hr, shown for 50ms.
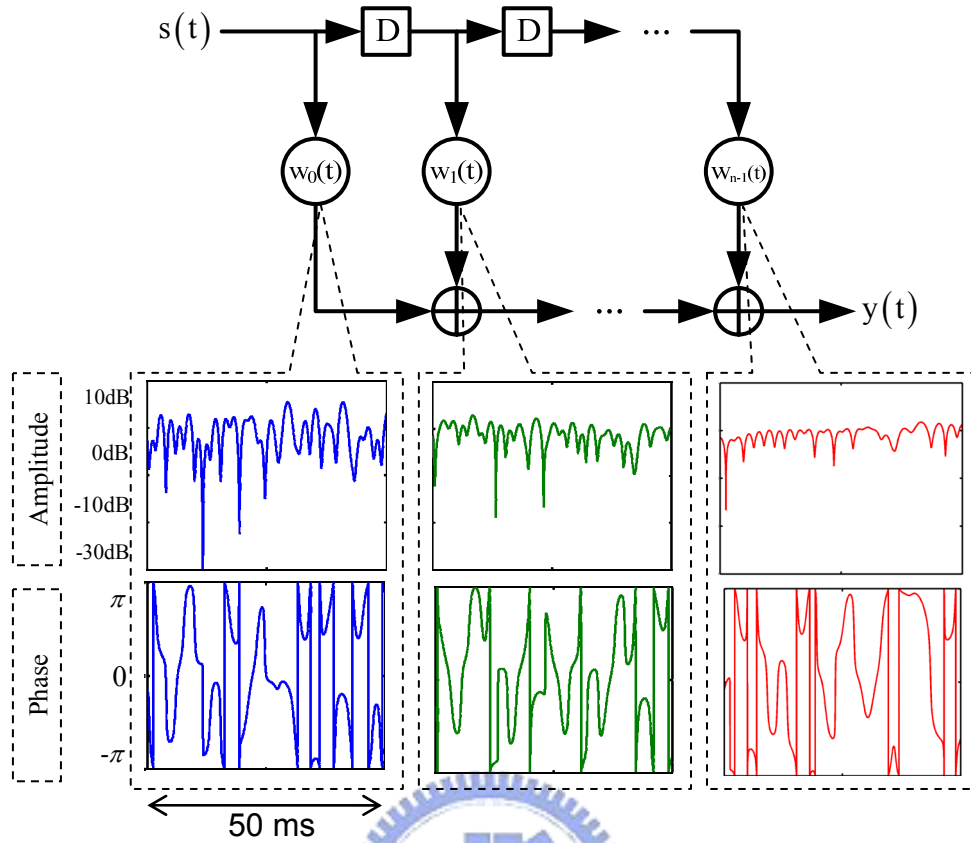
Figure 2-8: FIR filter with Rayleigh-distributed tap gains at 120km/hr

Where $s(t)$ is the transmitted signal and the received signal $y(t)$ can be written as a convolution sum

$$y(t) = \sum_{k=0}^{n-1} w_k(t)^* \cdot s(t-k) \tag{2.2}$$

The Rayleigh-distributed tap gains $w_k(t)$ can be expressed as the sum of sinusoids [11], that is

$$w_k(t) = X_c(t)\cos 2\pi f_c t \; + \; X_s(t)\sin 2\pi f_c t$$

$$X_c(t) = 2\sum_{n=1}^{N_o} \cos\beta_n \cos 2\pi f_n t \; + \; \sqrt{2}\cos\alpha\cos 2\pi f_m t \tag{2.3}$$

$$X_s(t) = 2\sum_{n=1}^{N_o} \sin\beta_n \cos 2\pi f_n t \; + \; \sqrt{2}\sin\alpha\cos 2\pi f_m t$$

Where f_c is the carrier frequency, and it equals to 2.4GHz in 802.11n. f_m is the maximum Doppler frequency shift described as

$$f_D \approx \frac{v}{\lambda} \cdot \cos\theta \tag{2.4}$$

for $\theta = 0$. N_o is the number of oscillators that generate the sinusoid waveforms of angular frequency β_n. Detail description of the sum of sinusoids is referred to [11].

2.3.4 Carrier Frequency Offset

Carrier Frequency Offset (CFO) is caused by the local oscillators' inconsistency between the transmitter and receiver. The received signals $y(t)$ can be written as

$$y(t) = \sum_t s(t) \times e^{i2\pi\Delta ft + \theta} \tag{2.5}$$

Where Δf and θ are the differences of carrier frequency and carrier phase between TX and RX, respectively. CFO will cause the constellation of the transmitted signal become a circle, that means phase of the transmitted signal will rotate with time.
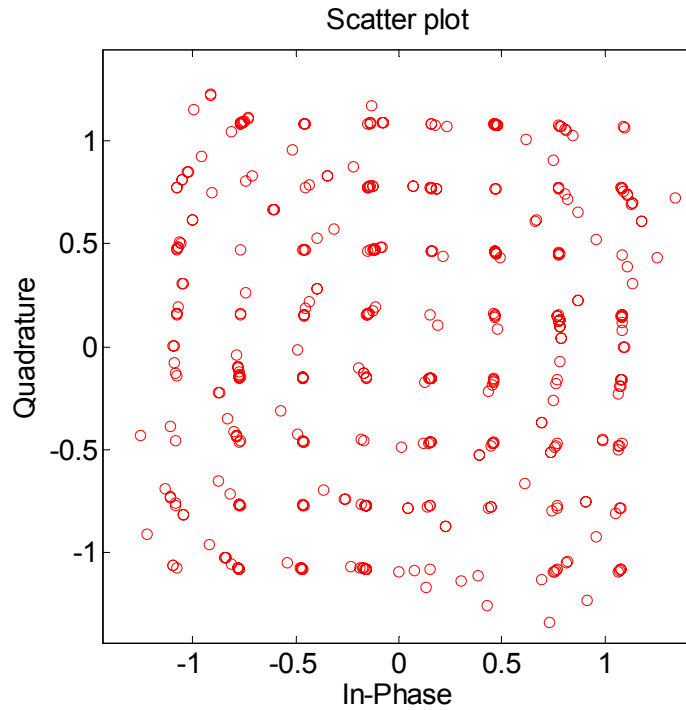
Figure 2-9: CFO effect under CFO 100 ppm use 64 QAM modulation

2.3.5 System Clock Offset

The clock drift means the different between the sampling frequency of the digital to analog converter (DAC) and the analog to digital converter (ADC). Because of

sampling frequency offset, even if the initial sampling point is optimized, the following sampling points will still slowly shift with time. This model is using compress sinc waveform to cause the clock drift effect, and its effect can be written as

$$R(nT_s) = R_{preADC}(nT_s) * \sin c(\frac{nT_s - \Delta T_n}{T_s}) \tag{2.6}$$

where R_{preADC} represents the ADC original output signal, ΔT_s represents shift sampling period and to get $R(nT_s)$ signal by convoluting the ADC original output signal and shifted sinc waveform. Figure 2-10 shows the clock drift model effect. Initial can samples at optimum sampling points, then slightly incorrect sampling instants will cause the SNR degradation.
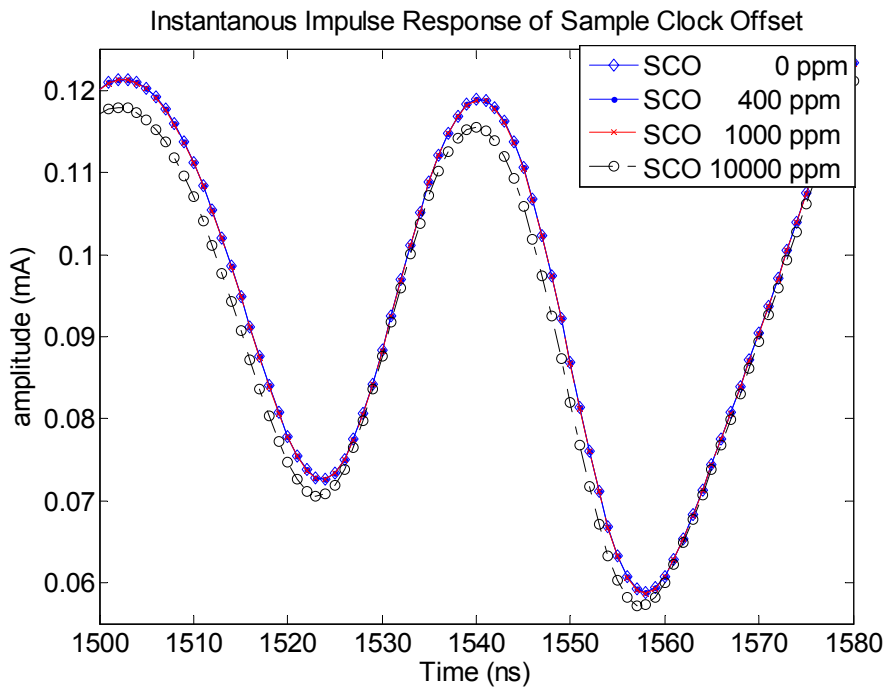
Figure 2-10: The sinc waveform of clock drift model effect

2.3.6 Impulsive Interference

Impulsive interference is a variety of naturally occurring and man-made phenomena exhibit impulsive behavior. A sentence that summarizes the chaotic nature of impulsive interference is "no two impulsive events are the same". There are many potential sources of impulsive interference [12]:

1. House appliances (washing machine, dish washer, food mixer, iron, oven, kettle, electric razor, drill, microwave oven, etc.).
2. Central heating thermostats.
3. Light switches (fluorescent, incandescent, etc.).
4. Ignition systems (traffic, lawn mower, etc.).

Based on [12], [13], [14], a set of impulsive interference models are modeled as a train of pulses.

$$n(t)=\sum_i A_i P_{w_i}(t-\tau_i) \tag{2.7}$$

where the amplitude A_i, duration W_i and arrival time τ_i of each pulse is a random variable whose distribution is a priori unknown.
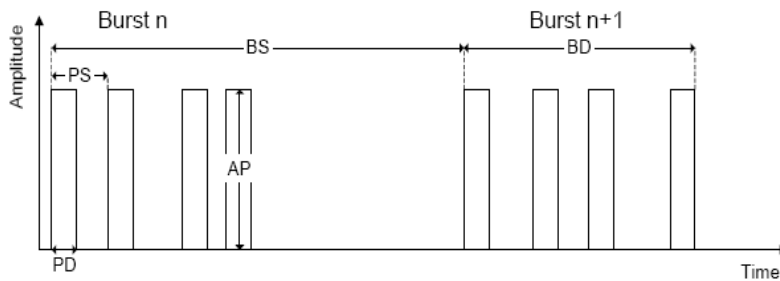
Figure 2-11: Parametric model for impulsive interference
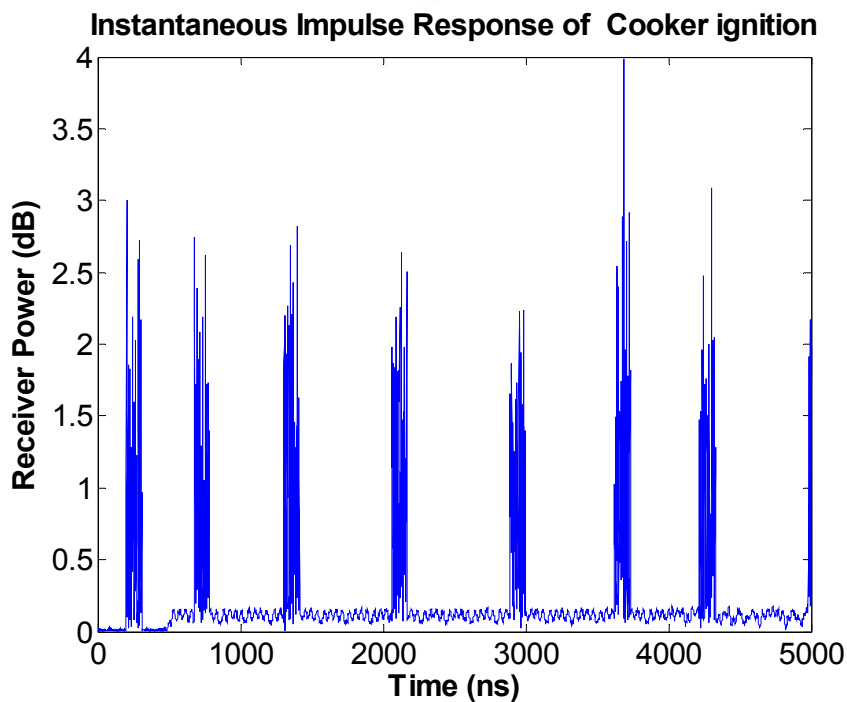
Figure 2-12: Interference impulsive model of Cooker ignition

Chapter 3

Proposed Algorithm

I N this chapter, a synchronization algorithm is proposed. The 4*4 MIMO-OFDM system with complicated channel model is aimed. The proposed synchronization scheme is shown in Figure 3-1.

The packet synchronization, it contains two parts: packet detection and symbol boundary detection, which simultaneously perform the correlation and detection is shown in the section 3.1. While doing the packet detection, the symbol boundary detection must be done to determine the starting of the symbol. The packet synchronization only uses first two preambles.

In section 3.2, the timing synchronization which gets the boundary coefficients form symbol boundary detection uses only one preamble (the third L-STS) by the sharing resource scheme. One symbol locked sampling acquisition, which measures received power under different sampling phases, is proposed not only to achieve the half sampling rate with large tolerant range, but also to get a "good" sampling phase.
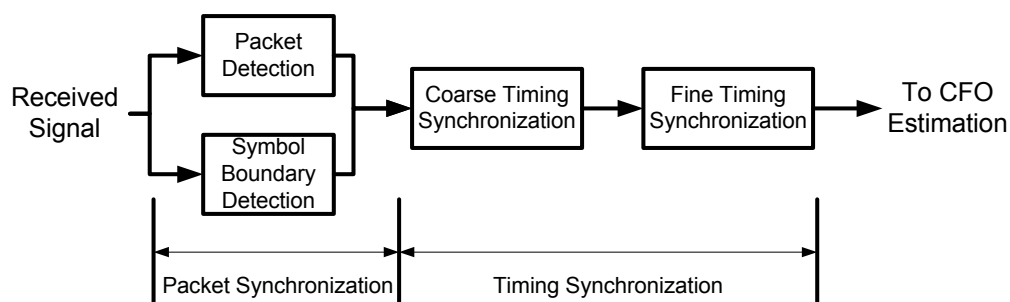
Figure 3-1: The proposed Synchronization Flow

3.1 Packet Synchronization

3.1.1 Packet Detection

3.1.1.1 Decision Variable

Consider with the AWGN channel first, we denote the k_{th} transmitted signal from the j_{th} transmit antenna as $S_j(k)$, the k_{th} received time domain signal at the i_{th} receive antenna as $R_i(k)$, and the additive white Gaussian noise between the j_{th} transmit antenna and the i_{th} receive antenna as N_{ij}. When a transmitted signal is presented

$$R_i = S_j(k) + N_{ij} \tag{3.1}$$

otherwise,

$$R_i(k) = N_{ij} \tag{3.2}$$

As pointed out before, L-STS can be used for packet detection. Because of the preamble has a repetitive structure, auto-correlation method will produce a useful decision statistic.

Based on algorithm in [9], assume the preamble repeats itself every L samples, the auto-correlation between the first and second L samples is

$$C(k) = \sum_{k=0}^{L-1} R_i(k-L+1) * R_i(k) \tag{3.3}$$

The received power for the second L samples is

$$P(k) = \left| \sum_{k=0}^{L} R_i(k) \right|^2 \tag{3.4}$$

And the decision variable on the i_{th} receive antenna is

$$u_i = \frac{|C(k)|^2}{|P(k)|^2} \tag{3.5}$$

Based on L received samples, we compared three methods to combine u_i to a stable u:

A. Mean method:

$$u = g_1(u_1, u_2, u_3, u_4) = \frac{1}{4} \sum_{i=0}^{4} u_i \qquad (3.6)$$

B. Geometric mean method:

$$u = g_2(u_1, u_2, u_3, u_4) = \frac{1}{4} \sqrt{\prod_{i=0}^{4} u_i} \qquad (3.7)$$

C. Root-mean-square method:

$$u = g_3(u_1, u_2, u_3, u_4) = \sqrt{\frac{1}{4} \sum_{i=0}^{4} u_i^2} \qquad (3.8)$$

| A. Mean method | B. Geometric mean method | C. Root-mean-square method |
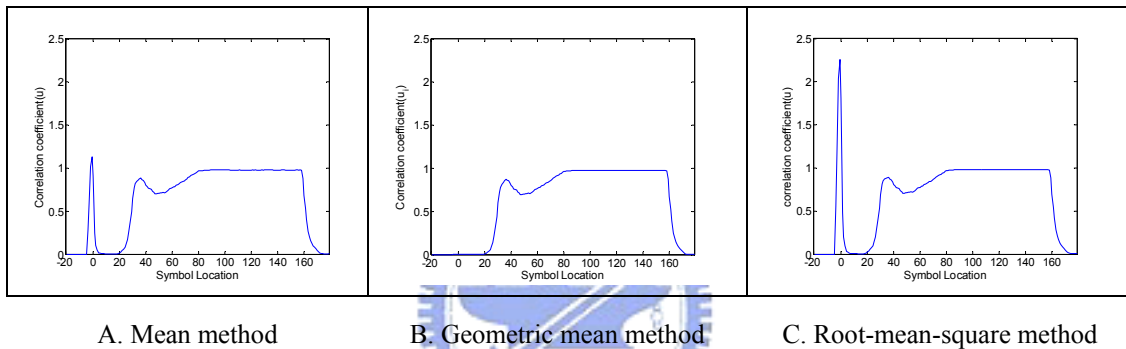
Figure 3-2: u_i distribution under different method

The result of different method under the same channel condition is shown in Figure 3-2. Before a packet is detected, those are called leading noises. Symbol location defines the different of signal and noise, in general positive means signal is presented and negative means noise is presented.

At symbol location is zero, the (2L-1) samples are all noises except the least one. Both mean and RMS method have unexpected peak which may cause by correlation buffer full of both noises and signal. It will make packet detection complexity higher and less reliable. As a result, the geometric mean method is chose.

3.1.1.2 Detection Algorithm

The set of samples $f_i(R_i(k-L+1), R_i(k-L+2), R_i(k-L+3), ... R_i(k))$ formed the decision variable u_i is depend on the decision window of size L. The decision variable u is calculate by the four u_i. Finally the u is compared to a preset

threshold u_{Th} in the following hypothesis test:

H_1, packet is present if $u > u_{Th}$;

H_2, packet is not present if $u \le u_{Th}$.

We stack the received signal for 2L samples, use equation (3.7) to calculate u. At the beginning of packet detection, we start with the state *No Peak.* If H_1 is true, the state change to *Finding Maximum Peak.*

There are two cases in the state *Finding Maximum Peak.* One is that if H_1 is true, every time u exceeds the threshold u_{Th} the *peak count* will increase by 1, and once if *peak count* exceeds the threshold $Peak_{Th}$, which means packet is already detected, the state change to *End Detection.* The other is that once H_2 is true, the state change to *Temporary* accordingly.

In the state *Temporary,* if H_2 is true, every time u under the threshold u_{Th} the *no peak count* will increase by 1, and once if *no peak count* exceeds the threshold $NoPeak_{Th}$, which means packet is not presented (it might be noise or interference impulsive), the state change back to *No Peak.* On the other hand, if H_1 is true, the state change to *Finding Maximum Peak* and reset some parameters which includes *peak count* and *no peak count* to zero.
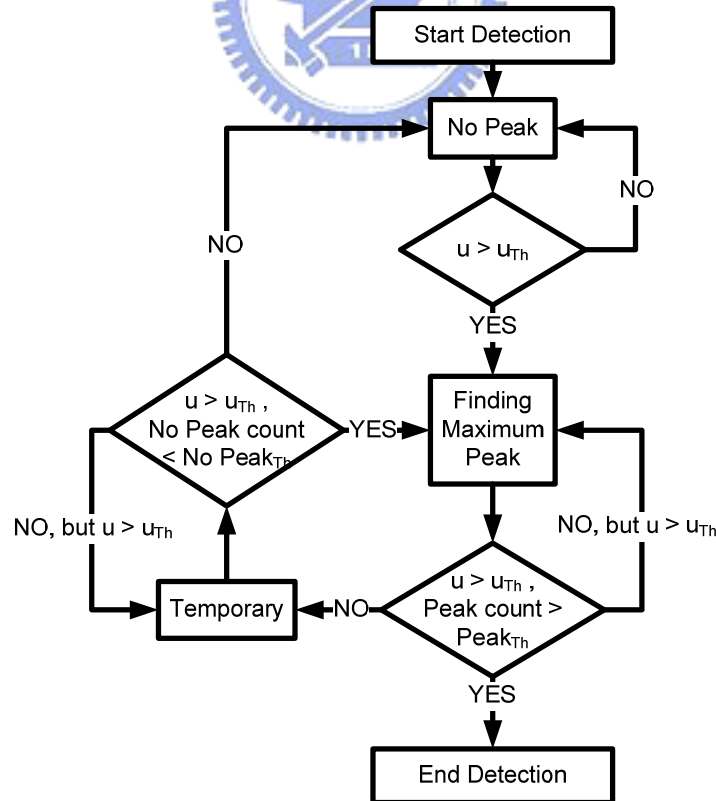
Figure 3-3: The flow chart of the packet detection algorithm.

3.1.2 Symbol Boundary Detection

3.1.2.1 Definition

In an OFDM system, P_L complex signal symbols are modulated onto P_L sub-carriers by using the inverse fast Fourier transform (IFFT) on the transmitter side. The last Pc IFFT samples are used to form a guard interval (GI) that is inserted at the beginning of each OFDM symbol.
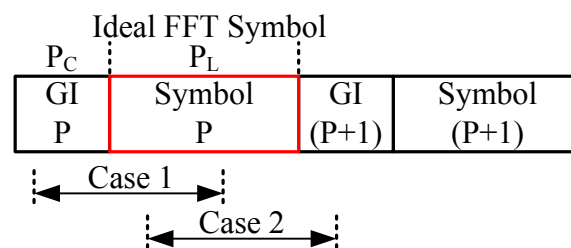
Figure 3-4: FFT symbol window

The misplaced FFT window can cause two different kinds of behaviors. First, the misplaced FFT window including the parts of the GI of the symbol is the case 1 as shown in Figure 3-4. In this case, the Pth FFT window has reordering alignment that means cyclic shift in time domain. It will produce frequency error in frequency domain and this effect can be compensated by equalization [8]. Second, the misplaced FFT window is the case 2 as shown in Figure 3-4, the Pth FFT window not only has the current symbol P but also includes a part of GI^{P+1}. In this case, the Pth FFT window has information lose, and the GI^{P+1} will cause inter-symbol interference (ISI) which cannot be recovered.

After the packet detection has provided an estimate of the start point of the packet, the symbol timing algorithm revise the estimate precision to achieve sample level which align the correct position of FFT symbol.

3.1.2.2 Detection Algorithm

First, we get the 2L samples of received signal for packet detection. In the other word, when a packet is presented change to the state **End detection**, while using those 2L samples of received signal in correlation buffer. Generally, those samples are mixed with noise and a part of L_STS. Therefore, an appropriately u_{Th} is chose to

ensure using the specific number of L_STS in correlation buffer.

This refinement is performed by calculating the parallel cross-correlation of the received signal $R_i(k)$ and the known short training sequence $Q(k)$ to be reference. Figure 3-5 shown the proposed symbol boundary detection architecture, the algorithm includes 6 steps:

Step 1. By using the repetitive property of L_STS, we define a L x B matrix of $Q(k)$ which consists of $Q_L(k)$.

$$Q(k) = \begin{bmatrix} Q_1(k) \\ Q_2(k) \\ Q_3(k) \\ \vdots \\ Q_{L-2}(k) \\ Q_{L-1}(k) \\ Q_L(k) \end{bmatrix} = \begin{bmatrix} L-STS(1) & L-STS(2) & L-STS(3)\cdots & \cdots & \cdots L-STS(B-2) & L-STS(B-1) & L-STS(B) \\ L-STS(16) & L-STS(1) & L-STS(2)\cdots & \cdots & \cdots L-STS(B-3) & L-STS(B-2) & L-STS(B-1) \\ L-STS(15) & L-STS(16) & L-STS(1)\cdots & \cdots & \cdots L-STS(B-4) & L-STS(B-3) & L-STS(B-2) \\ \vdots & \vdots & \vdots & \ddots & \vdots & \vdots & \vdots \\ \vdots & \vdots & \vdots & \ddots & \vdots & \vdots & \vdots \\ \vdots & \vdots & \vdots & \ddots & \vdots & \vdots & \vdots \\ L-STS(4) & L-STS(5) & L-STS(6)\cdots & \cdots & \cdots L-STS(B+1) & L-STS(B+2) & L-STS(B+3) \\ L-STS(3) & L-STS(4) & L-STS(5)\cdots & \cdots & \cdots L-STS(B) & L-STS(B+1) & L-STS(B+2) \\ L-STS(2) & L-STS(3) & L-STS(4)\cdots & \cdots & \cdots L-STS(B-1) & L-STS(B) & L-STS(B+1) \end{bmatrix}$$

(3.9)

Step 2. An appropriate correlation window size B is chose and it must be smaller than the packet detection correlation window L.

Step 3. The parallel cross-correlation with each $Q_L(k)$ indicate the correlation power $P_{i,L}(k)$.

$$\begin{aligned} P_{i,L}(k) &= p_i \left[R_i(k-B+1), R_i(k-B+2), R_i(k-B+3),...R_i(k) \right] \\ &= \left| \sum_{L=0}^{B} R_i(k-B+1) * Q_L(k-B+1) \right| \end{aligned}$$

(3.10)

Step 4. Use $P_{i,x}(k)$ to compute $\hat{Symbol}_{index}$ which is estimate symbol boundary index.

$$\hat{Symbol}_{index} = \arg\max_{L} \left\{ P_{i,L}(k) \right\}$$

(3.11)

Step 5. Combining the $\hat{Symbol}_{index}$ and the timing of packet detected; we can easily know the symbol timing and the right FFT symbol window.

Step 6. Using the correct symbol index, left and right neighbors that those provide for timing synchronization are defined as follow:

$$P_{i,D}(k) = \max\left(P_{i,L}(k)\right) \tag{3.12}$$

$$P_{i,D-1}(k) = P_{i,L-1}(k) \tag{3.13}$$

$$P_{i,D+1}(k) = P_{i,L+1}(k) \tag{3.14}$$
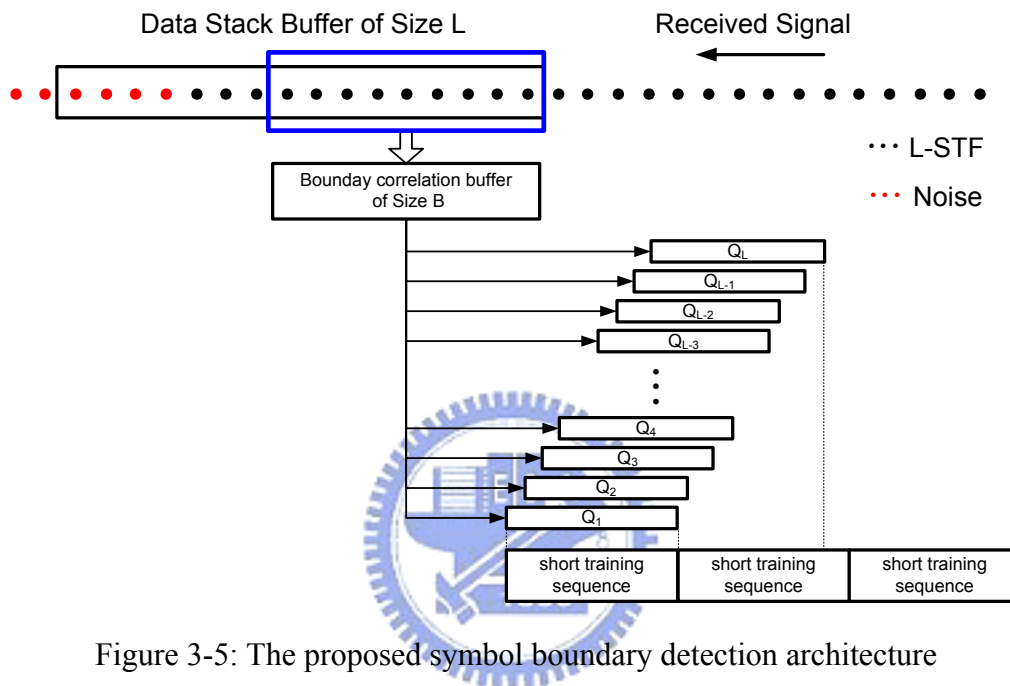
Figure 3-5: The proposed symbol boundary detection architecture

3.2 Timing Synchronization

3.2.1 Coarse Timing Synchronization

3.2.1.1 Basic Assumption

In this section, we introduce timing synchronization scheme. First, we consider with the boundary correlation buffer (BCB) fill with ideal short training sequence. We define $Q_1(k)$, $Q_2(k)$, and $Q_3(k)$ by equation (3.9), and set the BCB initial as $Q_2(k)$. From equation (3.10), $P_{i,1}(k)$, $P_{i,2}(k)$, and $P_{i,3}(k)$ are calculated. Proposed correlation architecture is shown as in Figure 3-6.

It apparent that $P_{i,2}(k)$ is much higher than $P_{i,1}(k)$ and $P_{i,3}(k)$ since the BCB

is exactly the same as $Q_2(k)$. $P_{i,1}(k)$ and $P_{i,3}(k)$ should be the same because of each of them has $B-1$ samples in common with $Q_2(k)$.
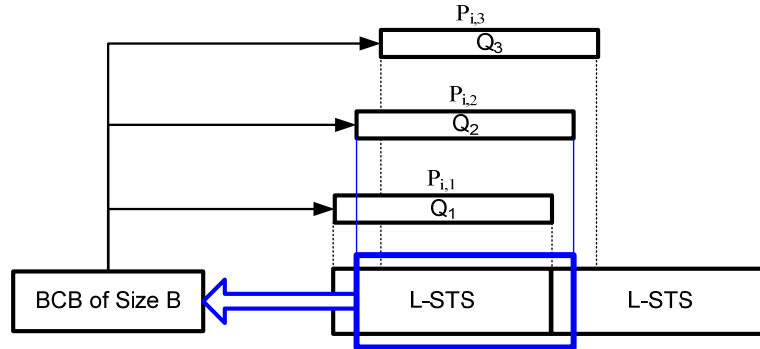
Figure 3-6: Proposed correlation architecture

On further consideration, we define ϕ_{ini} as phase error which might cause by channel effect like AWGN, mutipath, CFO, SCO …etc. When $\phi_{ini} = 2\pi$ means signal is misplaced for one sample (delay one sample). In other word, the signals inside BCB are exactly the same as $Q_3(k)$, and result in $P_{i,3}(k)$ become the highest one. When $\phi_{ini} = -2\pi$ also means that signal is misplaced for one sample (early one sample). Similarly, the signal inside BCB is exactly the same as $Q_1(k)$, and result in $P_{i,1}(k)$ become the highest one. The correlation between $P_{i,L}$ and phase error is shown as in Figure 3-7.

Take consideration with 4*4 MIMO-OFDM system with 64 QAM modulation and TGn channel E (RMS=100ns, Tap=15). The relation of boundary coefficients is shown in Figure 3-8. A multiphase generator is used to generate 22 phases.

Figure 3-7: Correlation between $P_{i,L}$ and Phase error
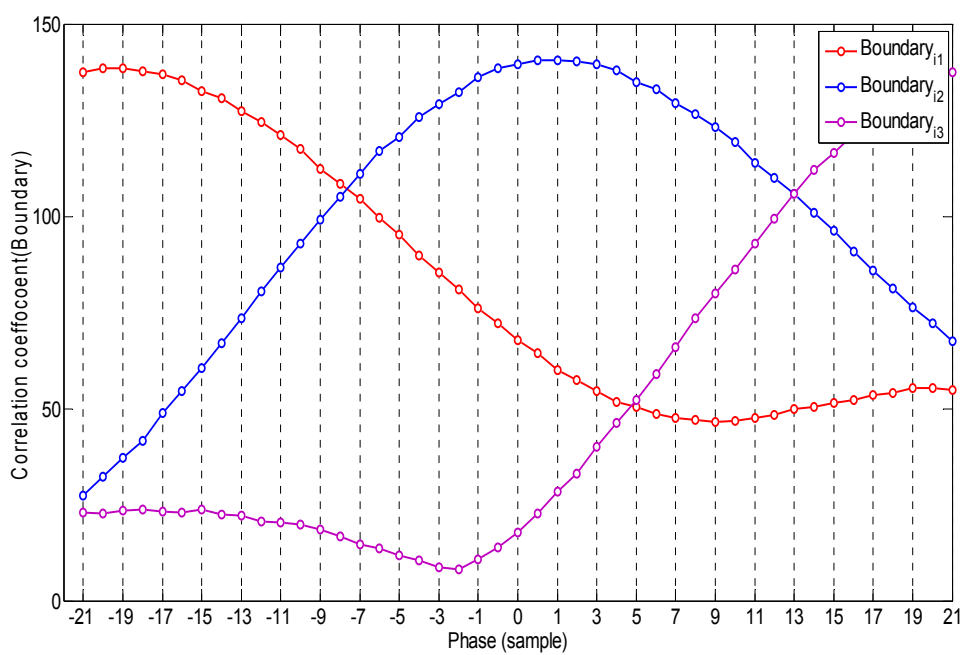
Figure 3-8: The boundary coefficient distribution (Packet no. = 1000)

3.2.1.2 Decision Region

As shown in Figure 3-7, different relationships between $P_{i,L}$ can be divided into four regions. The different condition of each region is described as follow:

Rough Forward (RF) Region: $P_{i,1}(k)$ is the highest one means the sampler sampled too early, $\phi_{ini} > -\pi$. In other word, we need to enlarge phase different of sample, equivalent to decrease sampling rate quickly. So that in this region we rotate the phase by π, $\phi_1 = \pi$.

Smooth Forward (SF) Region: $P_{i,2}(k)$ is the highest, and $P_{i,1}(k) > P_{i,3}(k)$, $0 > \phi_{ini} > -\pi$. In other word, we still need to enlarge phase different of sample, but to decrease sampling rate slowly. In this region we rotate the phase by $\frac{\pi}{2}$, $\phi_1 = \frac{\pi}{2}$.

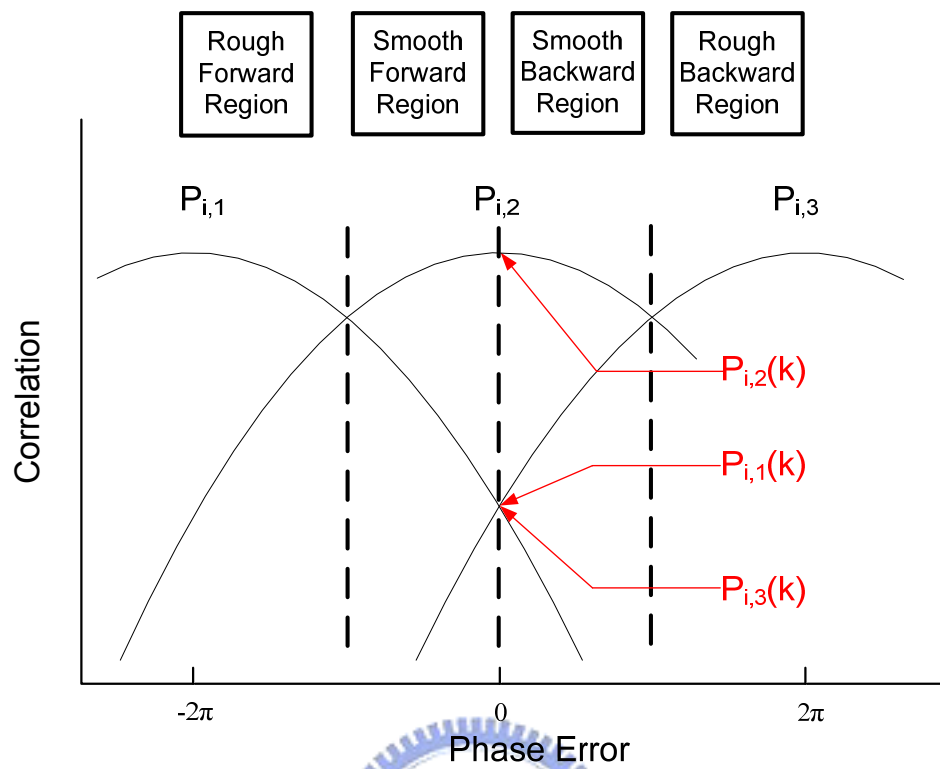**Smooth Backward (SB) Region**: $P_{i,2}(k)$ is the highest, and $P_{i,1}(k) \leq P_{i,3}(k)$, $0 < \phi_{ini} < \pi$. In other word, we need to narrow phase different of sample, equivalent to increase sampling rate slowly. In this region we rotate the phase by $-\frac{\pi}{2}$, $\phi_1 = -\frac{\pi}{2}$.

Rough Backward (RB) Region: $P_{i,3}(k)$ is the highest one means the sampler sampled too slow, $\phi_{ini} > \pi$. In other word, we still need to narrow phase different of sample, but to increase sampling rate quickly. So that in this region we rotate the phase by $-\pi$, $\phi_1 = -\pi$.

As mentioned before, after symbol boundary detection there are three boundary coefficients are passed to timing synchronization. Base on the relation of three boundary coefficients, a region is decided. The first rotation angle is decided by the region. After the rotation, the phase error will be:

$$\phi_{rot} = \phi_{ini} + \phi_1 = \phi_{ini} \pm \pi, \text{ if in Rough Region;}$$

$$\phi_{rot} = \phi_{ini} + \phi_1 = \phi_{ini} \pm \frac{\pi}{2}, \text{ if in Smooth Region.} \tag{3.15}$$

3.2.1.3 Decision Algorithm

After the first rotation, it came out three new $P_{i,L}$, named as $P\_rot_{i,L}$. These $P\_rot_{i,L}$ index a new region. By the regions of the two sets of boundary coefficients we estimation the phase error after rotated ϕ_{fin}.

From RF Region to RF Region:

In this case, it appears at $\phi_{ini} = -2\pi$ and after rotated π result in $\phi_{rot} = -\pi$ (see Figure 3-9). There still need one rotation to make phase error zero. $\phi_2 = \pi$, $\phi_{fin} = \phi_{rot} + \phi_2$.

Figure 3-9: From RF Region to RF Region diagram

From RF Region to SF Region:

In this case, as shown in Figure 3-10, initial phase had phase error ϕ_{ini} and $P_{i,L}$ located on red line, and after first rotation the phase became ϕ_{rot} and $P\_rot_{i,L}$ located on blue line. Assume $\phi_{rot} = -\phi_2$, and $\phi_{rot} = \phi_{ini} + \pi$, from the $P_{i,L}$ and the $P\_rot_{i,L}$ we can calculate the second rotation angle by followed equations:

$$\frac{\pi - \phi_2}{\phi_2} = \frac{P\_rot_{i,2} - P\_rot_{i,1}}{P_{i,1} - P_{i,2}} \tag{3.16}$$

$$\frac{\pi - \phi_2}{\pi} = \frac{P\_rot_{i,2} - P\_rot_{i,1}}{P\_rot_{i,2} - P\_rot_{i,3}} \tag{3.17}$$

$$\phi_2 = \left(\frac{P_{i,1} - P_{i,2}}{P\_rot_{i,2} - P\_rot_{i,3}} \right) \pi \tag{3.18}$$

Where $\phi_{fin} = \phi_{rot} + \phi_2$.

Figure 3-10: From RF Region to SF Region diagram

From SF Region to SF Region:

In this case, as shown in Figure 3-11, initial phase had phase error ϕ_{ini} and $P_{i,L}$ located on red line, and after first rotation the phase became ϕ_{rot} and $P\_rot_{i,L}$ located on blue line. Assume $\phi_{rot} = -\phi_2$, and $\phi_{rot} = \phi_{ini} + \dfrac{\pi}{2}$, from the $P_{i,L}$ and the $P\_rot_{i,L}$, we can calculate the second rotation angle by followed equations:

$$\frac{\frac{\pi}{2} - \phi_2}{\pi - \phi_2} = \frac{P_{i,2} - P_{i,1}}{P\_rot_{i,2} - P\_rot_{i,1}} \tag{3.19}$$

$$\frac{\frac{\pi}{2} - \phi_2}{\pi} = \frac{2\left(P_{i,2} - P_{i,1}\right)}{(P_{i,2} - P_{i,3}) + (P\_rot_{i,2} - P\_rot_{i,3})} \tag{3.20}$$

$$\frac{\pi - \phi_2}{\pi} = \frac{2\left(P\_rot_{i,2} - P\_rot_{i,1}\right)}{(P_{i,2} - P_{i,3}) + (P\_rot_{i,2} - P\_rot_{i,3})} \tag{3.21}$$

$$\phi_2 = \frac{\pi}{2} - \frac{2\pi\left(P_{i,2} - P_{i,1}\right)}{(P_{i,1} + P_{i,3}) + (P\_rot_{i,1} + P\_rot_{i,3})} \tag{3.22}$$

$$= \pi - \frac{2\pi\left(P\_rot_{i,2} - P\_rot_{i,1}\right)}{(P_{i,1} + P_{i,3}) + (P\_rot_{i,1} + P\_rot_{i,3})}$$

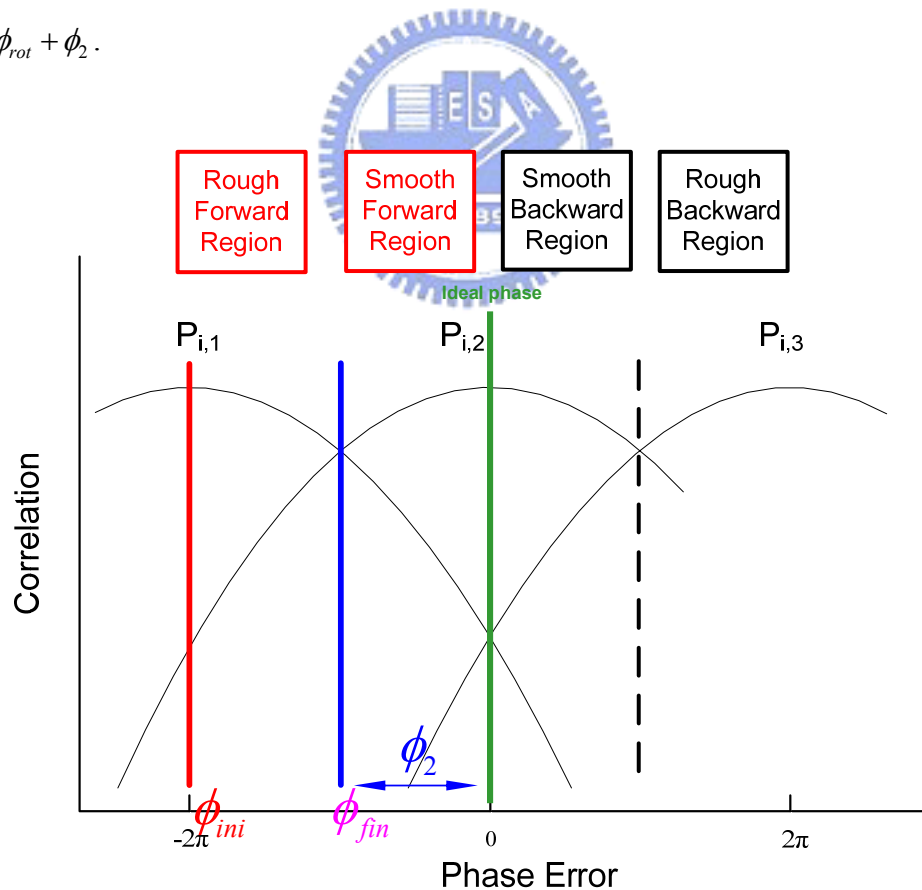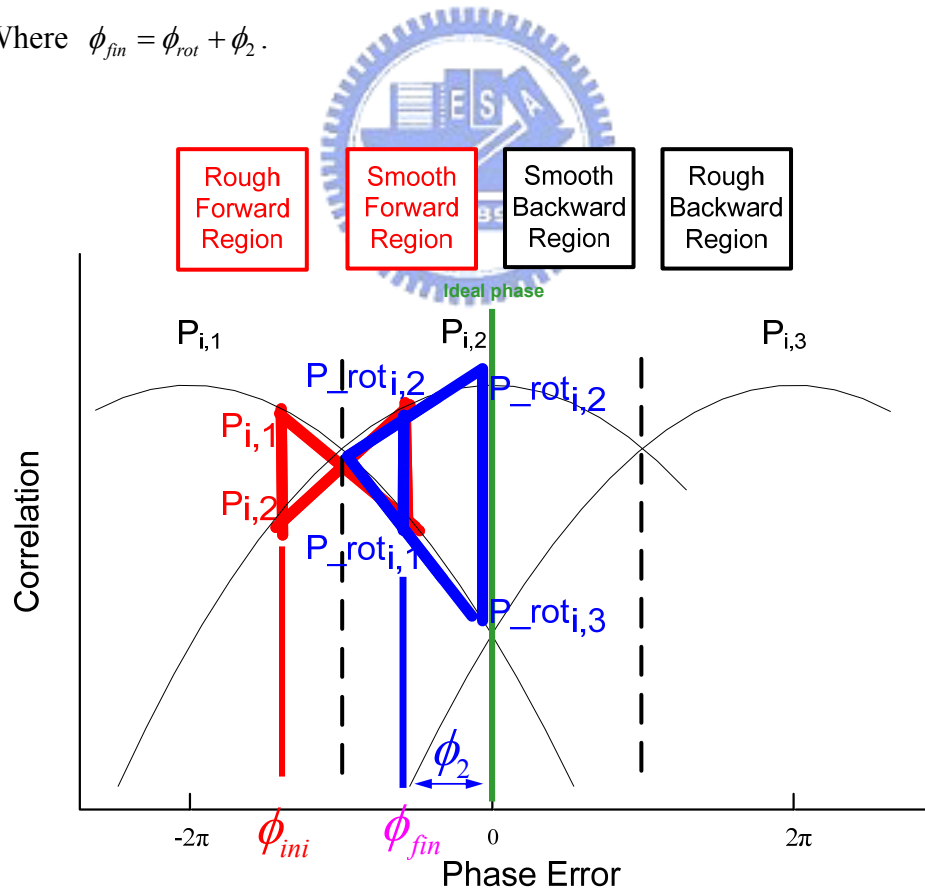Where $\phi_{fin} = \phi_{rot} + \phi_2$.
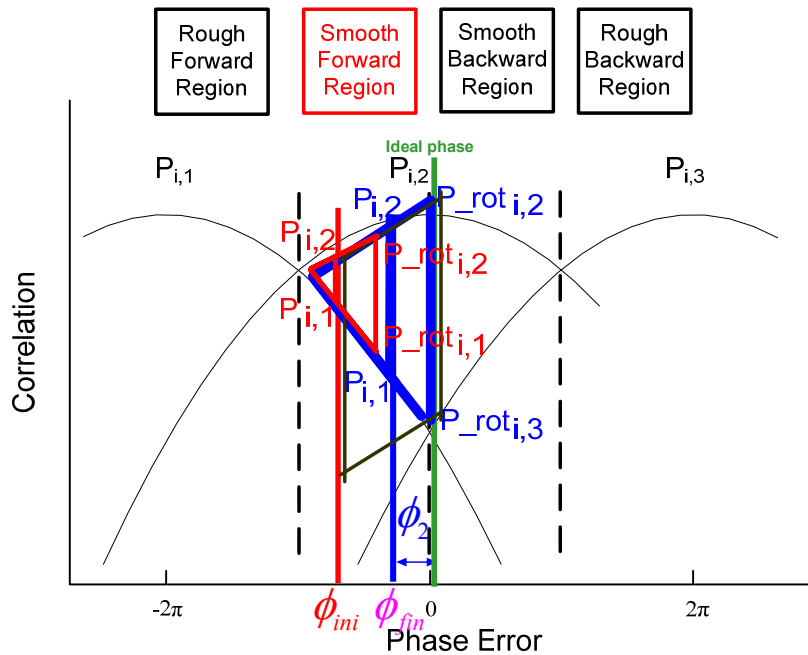
Figure 3-11: From RF Region to SF Region diagram

From SF Region to SB Region:

In this case, as shown in Figure 3-12, initial phase had phase error ϕ_{ini} and $Boundary_{ix}$ located on red line, and after first rotation the phase became ϕ_{rot} and $Boundary\_rot_{ix}$ located on blue line. Assume $\phi_{rot} = \phi_2$, and $\phi_{rot} = \phi_{ini} + \dfrac{\pi}{2}$, from the $Boundary_{ix}$ and the $Boundary\_rot_{ix}$ we can calculate the second rotation angle by followed equations:

$$\frac{\frac{\pi}{2} + \phi_2}{\pi} = \frac{2(P_{i,2} - P_{i,1})}{(P_{i,2} - P_{i,3}) + (P\_rot_{i,2} - P\_rot_{i,3})} \tag{3.23}$$

$$\frac{\pi - \phi_2}{\pi} = \frac{2(P\_rot_{i,2} - P\_rot_{i,1})}{(P_{i,2} - P_{i,3}) + (P\_rot_{i,2} - P\_rot_{i,3})} \tag{3.24}$$

$$\phi_2 = \frac{2\pi(P_{i,2} - P_{i,1})}{(P_{i,2} - P_{i,3}) + (P\_rot_{i,2} - P\_rot_{i,3})} - \frac{\pi}{2} \tag{3.25}$$

$$= \frac{2\pi(P\_rot_{i,2} - P\_rot_{i,1})}{(P_{i,2} - P_{i,3}) + (P\_rot_{i,2} - P\_rot_{i,3})} - \pi$$

Where $\phi_{fin} = \phi_{rot} - \phi_2$.
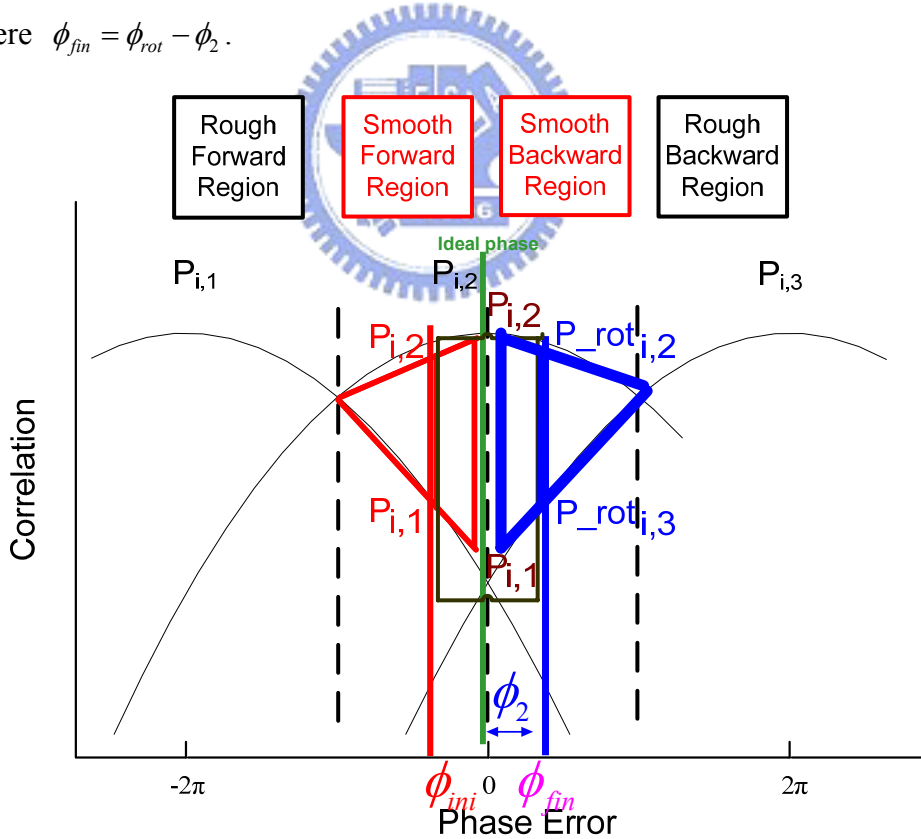
Figure 3-12: From RF Region to SF Region diagram

From SB Region to SF Region:

The ϕ_2 is the same as ϕ_2 in equation(3.25), but $\phi_{rot} = -\phi_2$.

From SB Region to SB Region:

The ϕ_2 is the same as ϕ_2 in equation(3.22), but $\phi_{rot} = \phi_2$.

From RB Region to SB Region:

The ϕ_2 is the same as ϕ_2 in equation(3.18), but $\phi_{rot} = -\phi_2$.

From RB Region to RB Region:

It appear at $\phi_{ini} = 2\pi$ and after rotated $-\pi$ result in $\phi_{fin} = \pi$.

The flow chart is shown in Figure 3-13. The first rotation depends on the initial region, and the second rotation depends on the calculation.
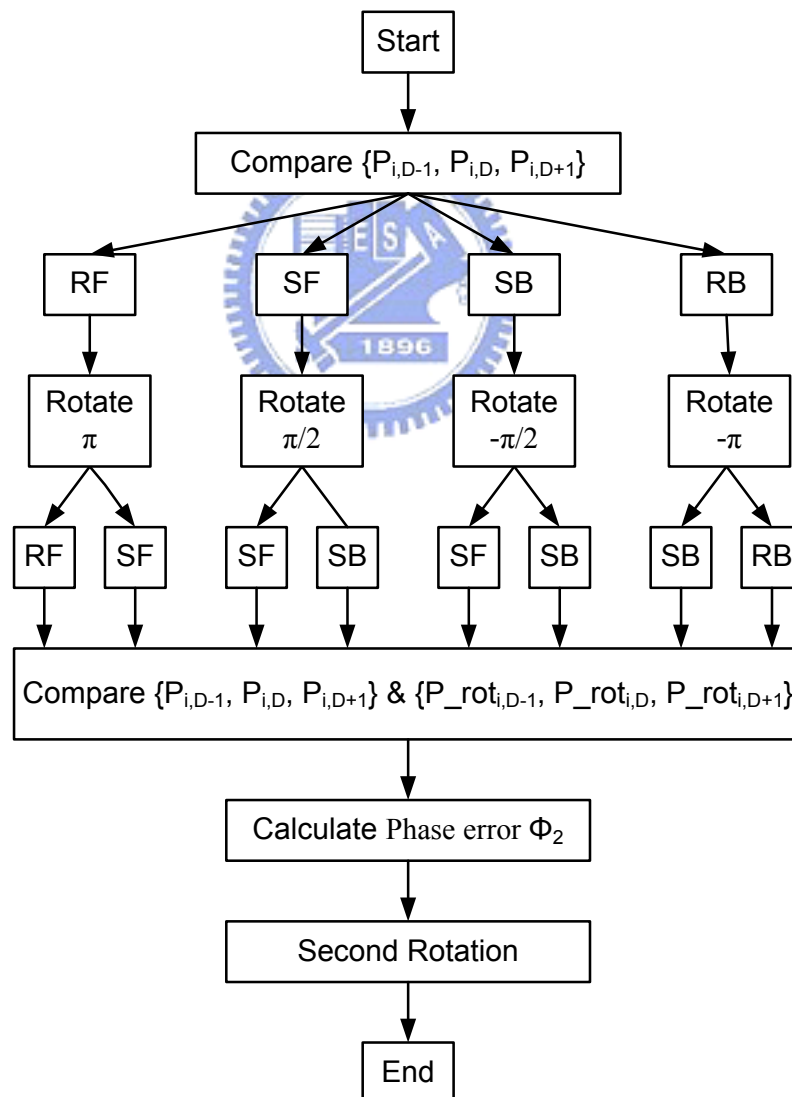
Figure 3-13: The flow chart of the proposed coarse timing synchronization

3.2.2 Fine Timing Synchronization

In real systems, channel effect is much complicated. The correlation between $P_{i,L}$ and phase error might not as smooth as the model, neither does the correlation between $P_{i,L}$ and $P\_rot_{i,L}$. To make a better phase error estimation, we need to do fine timing synchronization to confirm:

$$Rotated_D = g(P_{i,(D-1)}, P_{i,D}, P_{i,(D+1)})$$
$$= \sqrt{\prod_{i=0}^{4} \frac{P_{i,(D-1)} * P_{i,(D+1)}}{|P_{i,D}|^2}} \qquad (3.26)$$

$$\tilde{E}_{phase} = \arg\min_{x} \{Rotated\_ini_D, Rotated\_rot_D, Rotated\_fin_D\} \qquad (3.27)$$

As mention before, we have $Rotated\_ini_D$ with phase error ϕ_{ini}, $Rotated\_rot_D$ with phase error ϕ_{rot}, and $Rotated\_fin_D$ with phase error ϕ_{fin}. $Rotated_D$ is calculated to get $\tilde{E}_{phase}$ by equation(3.26). $\tilde{E}_{phase}$ finds the better phase which suppose to be $Rotated\_fin_D$ by three rotated value. If it is not, means we need to modify the estimated phase error ϕ_{fin}.
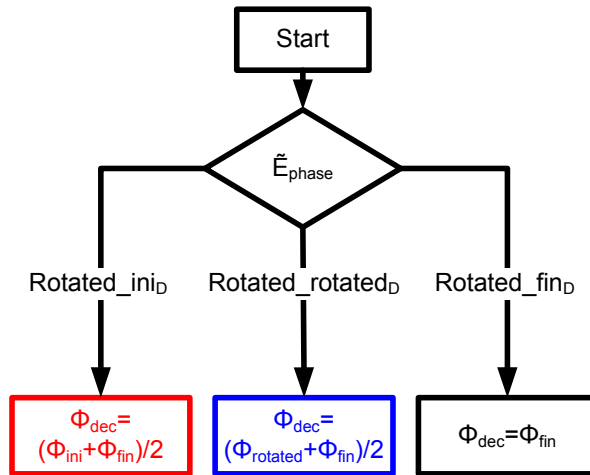
Figure 3-14: Modification of phase error ϕ_{fin}

Chapter 4

Simulation

$\mathbf{W}$E use simulation to evaluate the receiver's performance both in the AWGN channel and in a Rayleigh fading channel with additional channel effect. In the AWGN channel, as equation(3.1) mention before, $R_i = S_j(k) + N_{ij}$; On the other hand, in the Rayleigh fading channel with additional channel effect, we can express the received signal sample as:

$$R_i = \left(S_j(k) \otimes H_{ij}(\tau, k) \right) * e^{i(2\pi \Delta f t + \theta)} * \mathrm{sinc}(\frac{(k - \Delta T_n)n}{k}) + N_{ij}(k) + I_{ij}(k) \qquad (4.1)$$

Where the $H_{ij}(k)$ is the multipath with time-variant model, the exponential term is CFO effect, the sinc part is SCO effect, $N_{ij}(k)$ is AWGN, and $I_{ij}(k)$ is impulsive interference.

4.1 Simulation Platform

MATLAB is chosen as simulation language, due to its ability to mathematics, such as matrix operation, numerous math functions, and easily drawing figures. A MIMO-OFDM system based on IEEE 802.11n Wireless LANs, TGn Sync Proposal Technical Specification [7], is used as the reference simulation platform. The major parameters are shown in Table 4-1.

Table 4-1 Simulation parameters

Parameter	Value
MCS Set	27 / 29
Antenna No.	4*4
Modulation	16 QAM / 64 QAM
Coding Rate	2/3
PSDU Length	1024 Bytes
Carrier Frequency	2.4 GHz
Bandwidth	20 MHz
IFFT / FFT Period	3.2 μs

4.2 Simulation Result

4.2.1 Packet Synchronization Simulation Condition

In this section, the simulation environment is as follow:

Table 4-2 Packet synchronization simulation condition

Condition	Value
Packet No.	1000
Multipath	TGn E
RMS delay	100 ns
Tap No.	15
FDI	$\begin{bmatrix} 1 & 0.1 \\ 0.1 & 1 \end{bmatrix}$
CFO	50 ppm
SCO	50 ppm
T-variant	Jakes model
Velocity	60 km/hr
Interference	Cooker ignition
Burst Duration (pulses per burst)	20
Pulse Spacing	$1.5 \pm 0.5 \mu s$
SIR	-10 dB

4.2.1.1 Packet Detection

Figure 4-1 present the symbol location when packet detected under different SNR condition. The symbol location indicates the start of packet. A negative symbol location means packet is not present; there is only so-called leading noise.

When SNR<0, the packet detection shows false alarm, including detected at wrong time or detected when there is no packet, and the range of detection is too wide to be reliable. When SNR>0, the range of detection become narrow down to be acceptable one and the packet detection become more reliable.
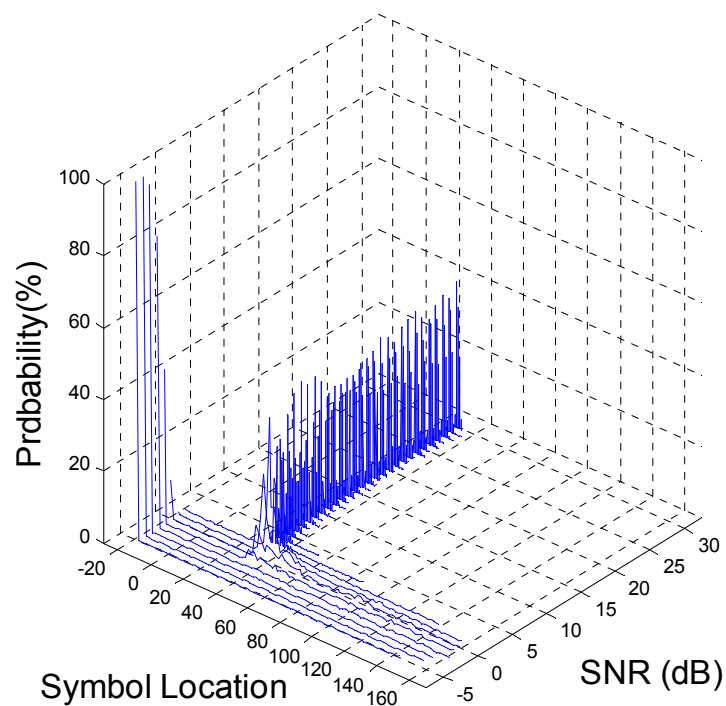

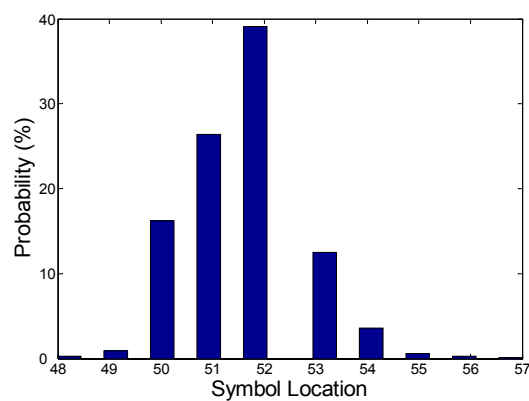Figure 4-1: Packet detection distribution versus different SNR

Figure 4-2: The probability of packet detection under SNR 0

4.2.1.2 Symbol Boundary Detection

Figure 4-3 present the sample location when packet detected under different SNR condition. The packet and the symbol boundary are detected simultaneously. Symbol location shows the packet start timing and similarly sample location help us to locate the symbol boundary. A multiphase generator is used to generate 22 different phases between one clock cycle, in other word, it means sample location is symbol location to multiply 22.

When SNR<5, because of the connection between packet detection and symbol boundary detection, symbol boundary detection suffer serious index errors due to packet detected errors, including packet loss (SNR<0) and packet detection false alarm (SNR<5) and weak signal power (as shown in Figure 4-4).

When SNR>5, the decrease of the packet detected errors result in the symbol boundary detection errors reduce apparently. We can also know from Figure 4-3 and Figure 4-4, the range of symbol boundary detection become narrow down to be acceptable one when SNR>5.

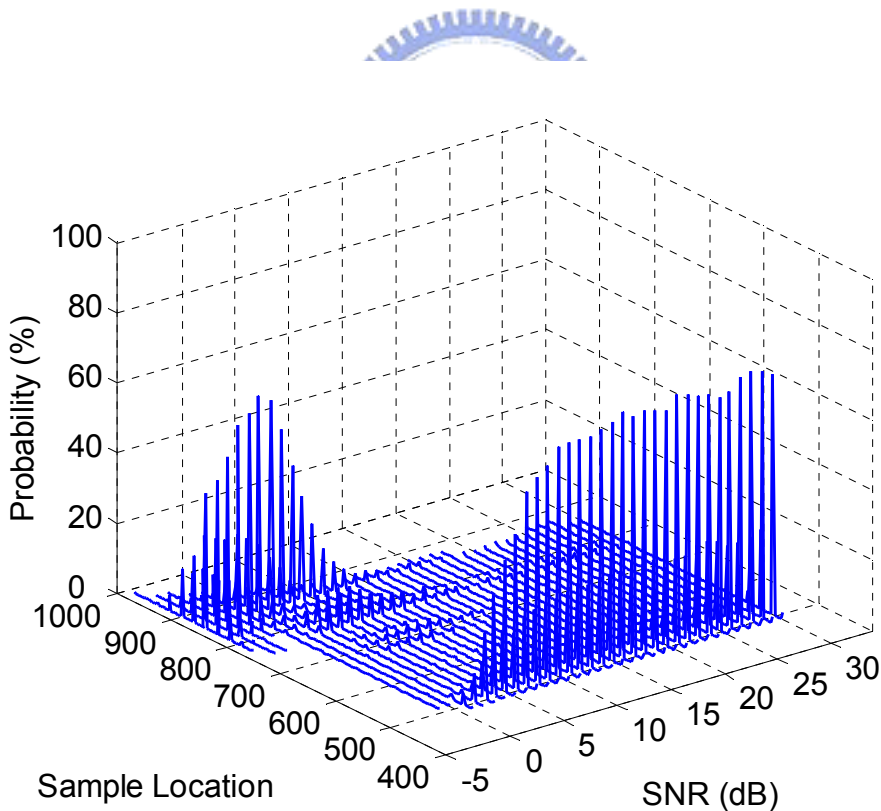Figure 4-3: Symbol boundary detection distribution versus different SNR
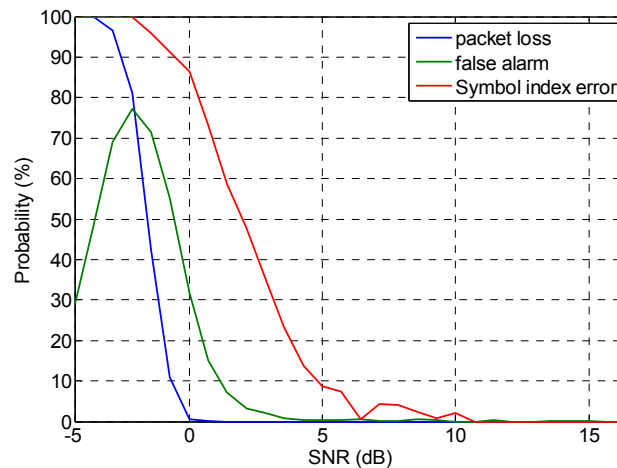
Figure 4-4: Symbol index error analysis

4.2.1.3 Packet Synchronization

Figure 4-5 present the system performance of packet synchronization with two different channel types. One is AWGN channel; it means the channel suffer from only AWGN. The other is complex channel; the condition of complex channel is described in section 4.2.1.

The legend "*Packet sync. on*" means the performance of the proposed packet synchronization algorithm. Relatively, "*Packet sync. off*" means the performance of the ideal packet synchronization, including ideal packet detection and ideal symbol boundary detection, that is, to know exactly the timing of packet start and send the exactly correct symbol into FFT.

In AWGN channel, the proposed algorithm and the ideal packet synchronization have the similar curves; they have almost the same performance. In Complex channel, although the curves are not smooth, basically they are still similar. Eventually the result in about 2.7dB lost when PER <0.1, but it may be cause by using too few packet numbers in the simulation.
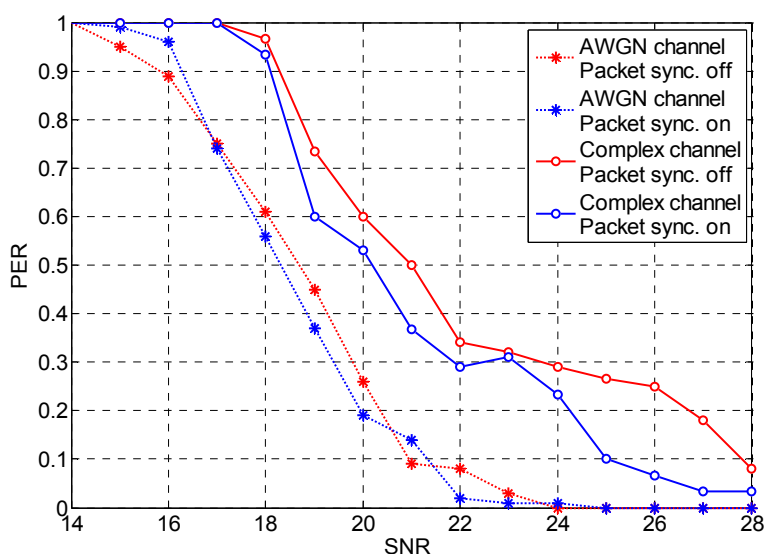
Figure 4-5: System performance of packet synchronization under AWGN and
Complex channels

4.2.2 Timing Synchronization

As mention before, the multiphase generator is used to generate 22 phases between one clock cycle. In other word, the phase error 22 means that signal is delay one cycle, and the phase error 0 means that sign is at ideal phase.

With different initial phase errors, after timing synchronization, including coarse and fine timing synchronization, the final phase errors are convergence into 2 phases. As shown in Figure 4-6.

Figure 4-6: The final phase errors with AWGN and Multipath (TGn E)

First, consider with the 4*4 MIMO-OFDM system with 16 QAM modulation and TGn channel D (RMS=50ns, Tap=8). The performances are shown in Figure 4-7.The legend *ideal sampling* means to get each sample at right phase (phase error 0). *One symbol locked sampling* means use the proposed algorithm in section 3.2 with an unknown initial phase errors to get sample.

Figure 4-7-(a) shows the required SNR for 10% PER is 16 dB, lost about 0.2 dB when compare with the ideal sampling. Take the SCO effect into consideration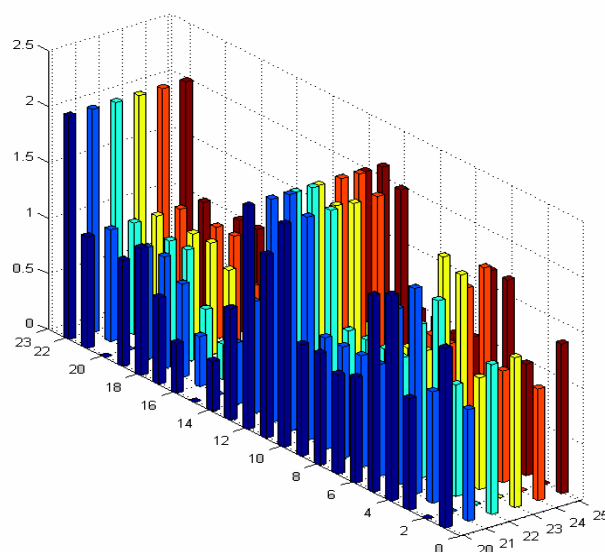, the required SNR for 10% PER with SCO 200 ppm is about 16.7dB, lost about 0.7 dB when compare with no SCO effect. Figure 4-7-(b) shows the proposed algorithm can tolerance SCO effect about 200 ppm.

Figure 4-8 present the performance of 4*4 MIMO-OFDM system with 16 QAM modulation and TGn channel E (RMS=100ns, Tap=15). Figure 4-8-(a) shows the required SNR for 10% PER is 25 dB, lost about 1.6 dB when compare with the ideal sampling. Take the SCO effect into consideration, the required SNR for 10% PER with SCO 200 ppm is about 27dB, lost about 2 dB when compare with no SCO effect. Figure 4-8-(b) shows the proposed algorithm can tolerance SCO effect about 200 ppm.

In Figure 4-8-(b) the required SNR for 10% PER with SCO 200 ppm is about 26dB, instead of 27 dB in Figure 4-8-(a). It could be cause by not enough packets since the curve is not smooth Figure 4-8-(a) or specific initial phase errors.

Then, consider with the 4*4 MIMO-OFDM system with 64 QAM modulation and TGn channel D (RMS=50ns, Tap=8). The performances are shown in Figure 4-9. Figure 4-9-(a) shows the required SNR for 10% PER is about 20.5 dB, lost about 0.8 dB when compare with the ideal sampling. Take the SCO effect into consideration, the required SNR for 10% PER with SCO 200 ppm is about 22dB, lost about 1.5 dB when compare with no SCO effect. Figure 4-9-(b) shows the proposed algorithm can tolerance SCO effect about 200 ppm.

Figure 4-10 present the performance of 4*4 MIMO-OFDM system with 64 QAM modulation and TGn channel E (RMS=100ns, Tap=15). Figure 4-10-(a) shows the required SNR for 10% PER is about 35 dB, lost about 2.8 dB when compare with the ideal sampling. Take the SCO effect into consideration, the required SNR for 10% PER with SCO 200 ppm is about 35.9 dB, lost about 0.9 dB when compare with no SCO effect. Figure 4-10-(b) shows the proposed algorithm can tolerance SCO effect about 200 ppm.
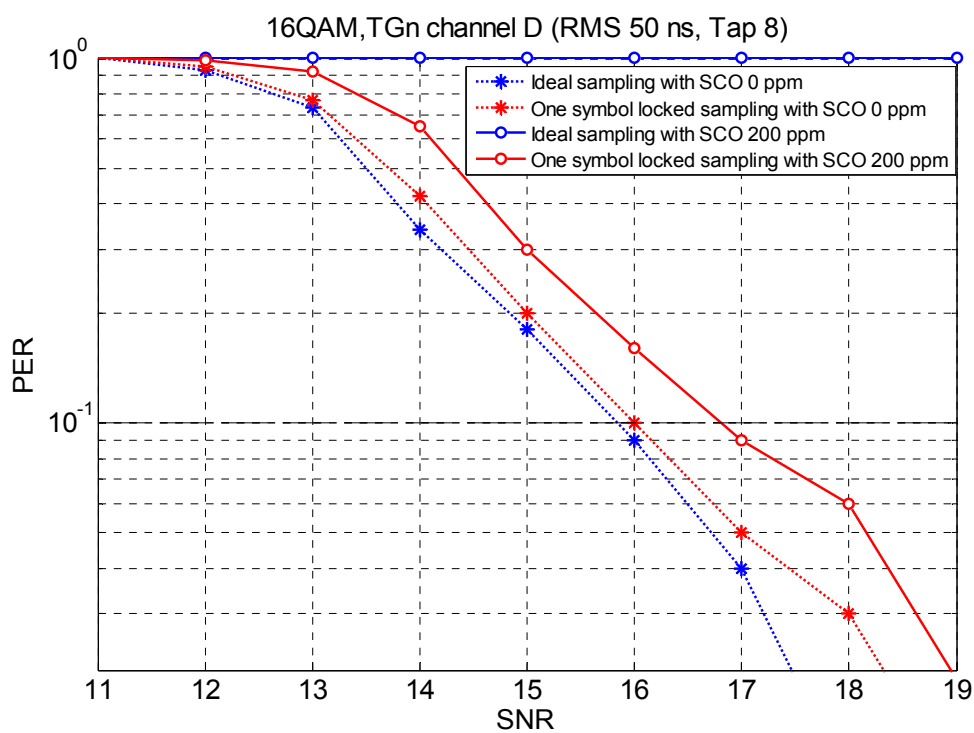
(a) PER vs. SNR
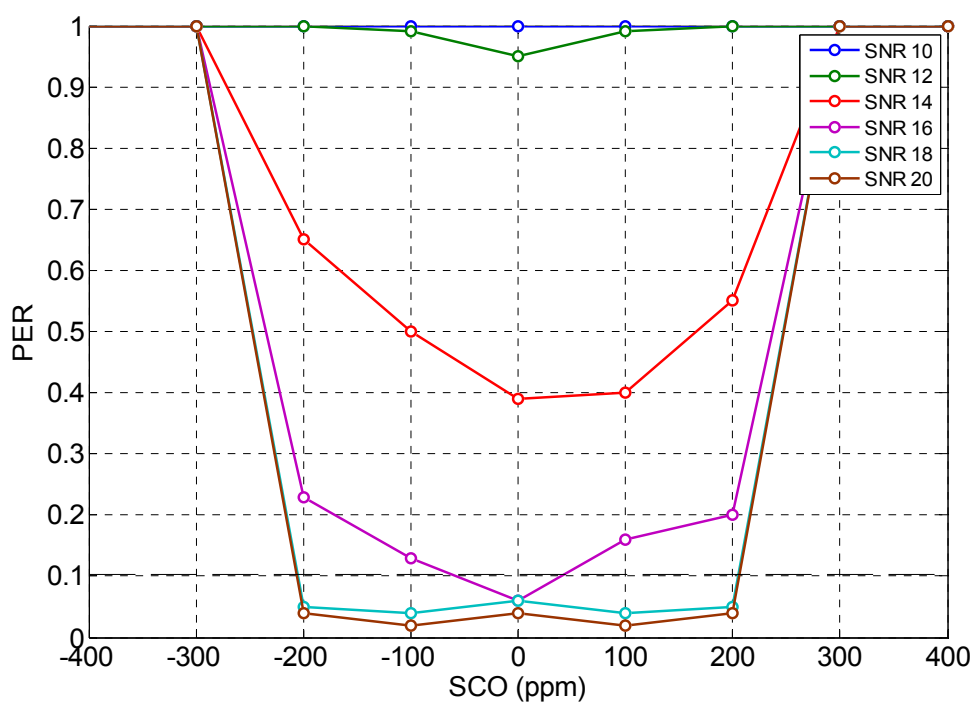
(b) PER vs. SCO

Figure 4-7: The system performance of 4*4 MIMO-OFDM with 16 QAM, TGn

channel D
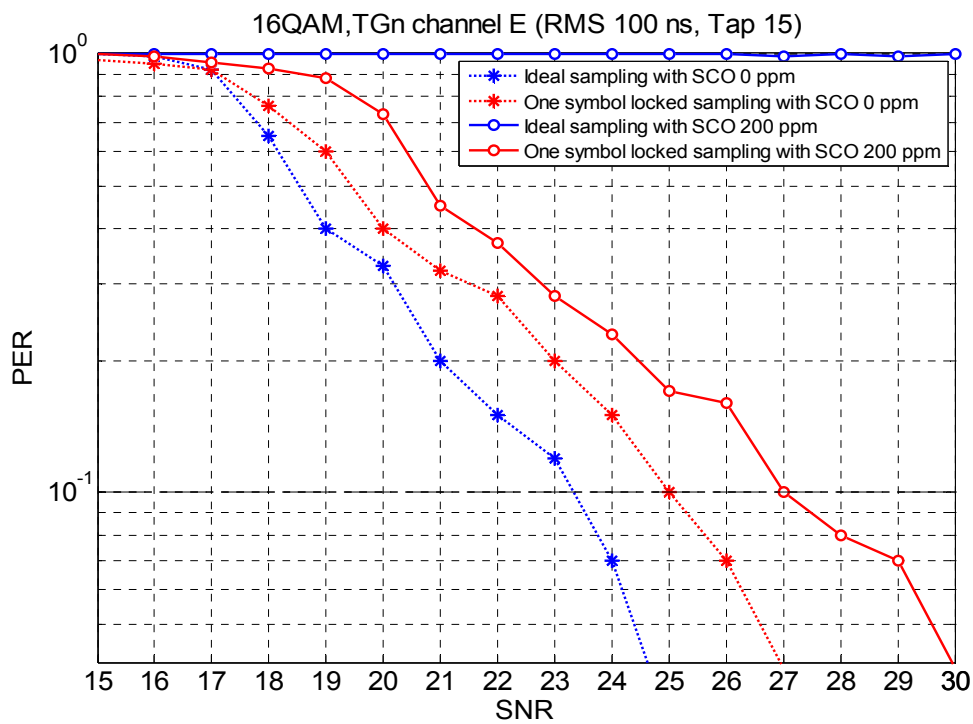
(a) PER vs. SNR
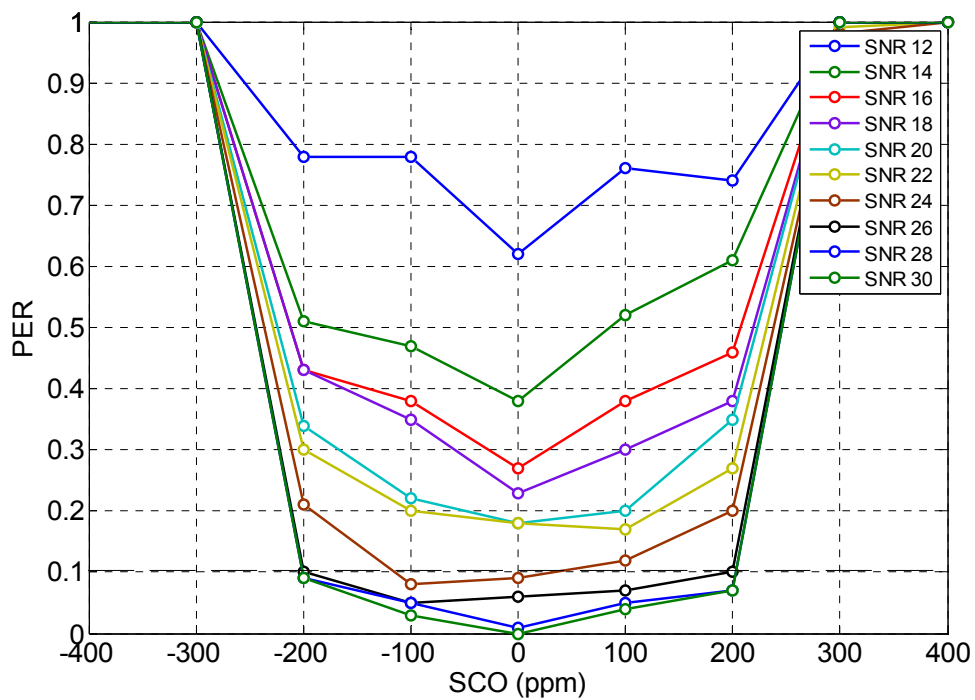
(b) PER vs. SCO

Figure 4-8: The system performance of 4*4 MIMO-OFDM with 16 QAM, TGn

channel E
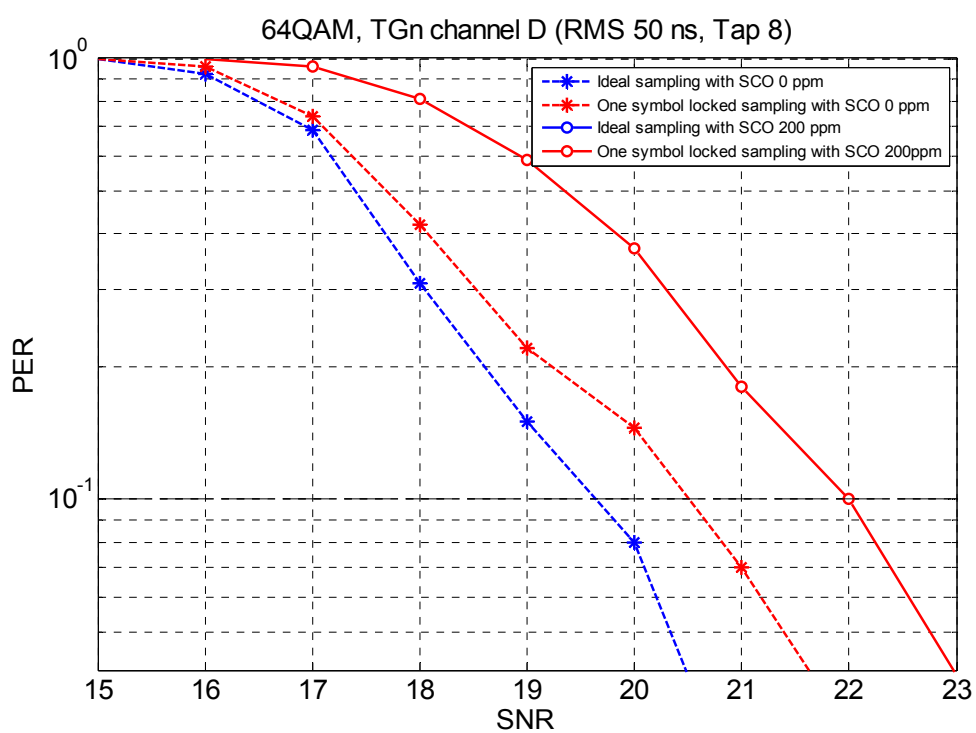
(a) PER vs. SNR
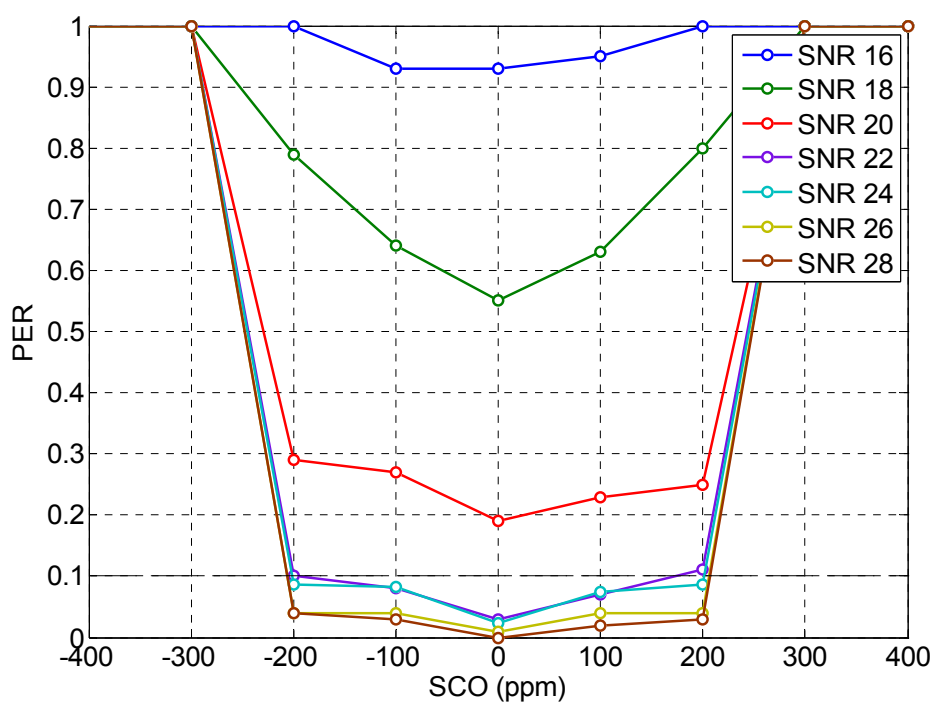
(b) PER vs. SCO

Figure 4-9: The system performance of 4*4 MIMO-OFDM with 64 QAM, TGn

channel D
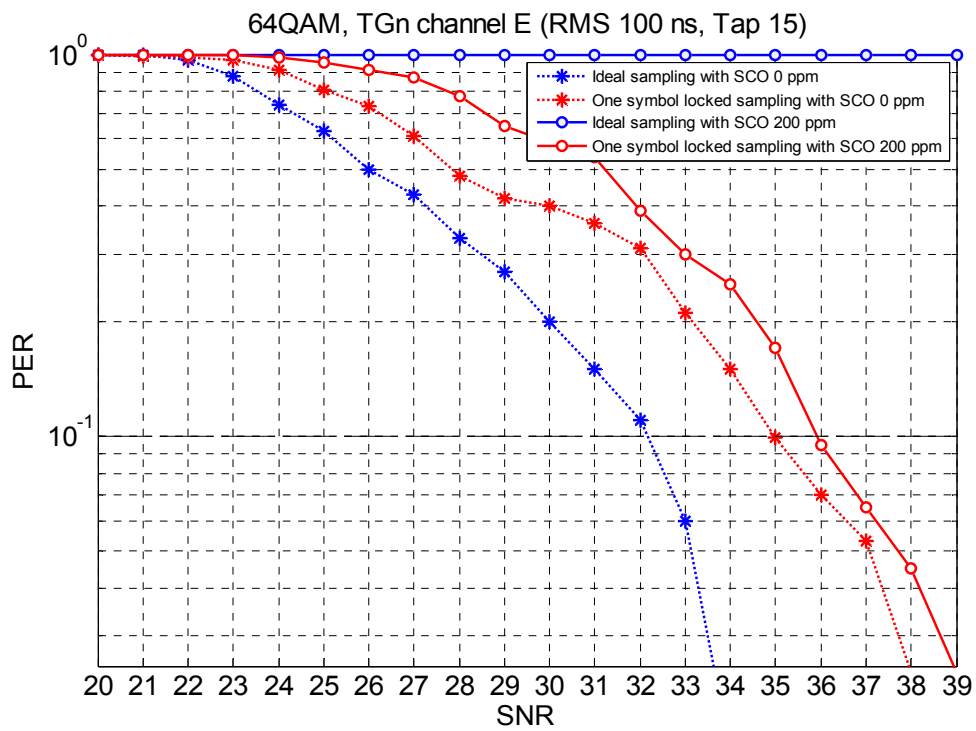
(a) PER vs. SNR
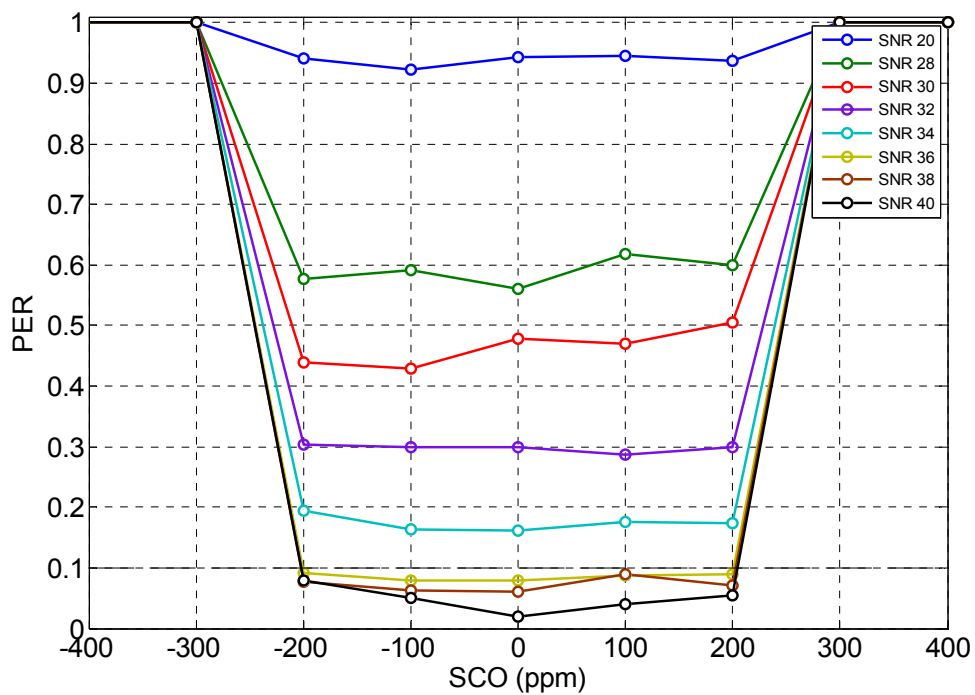
(b) PER vs. SCO

Figure 4-10: The system performance of 4*4 MIMO-OFDM with 64 QAM, TGn

channel E

Chapter 5

Hardware Implementation

A n synchronization scheme for 4*4 MIMO-OFDM systems is implemented. Section 5.1 gives the architecture of the 4×4 packet synchronization algorithm. The timing synchronization scheme is described in section 5.2. The hardware specifications, area report and power report of the proposed 4×4 synchronization algorithm are summarized in section 5.3 .
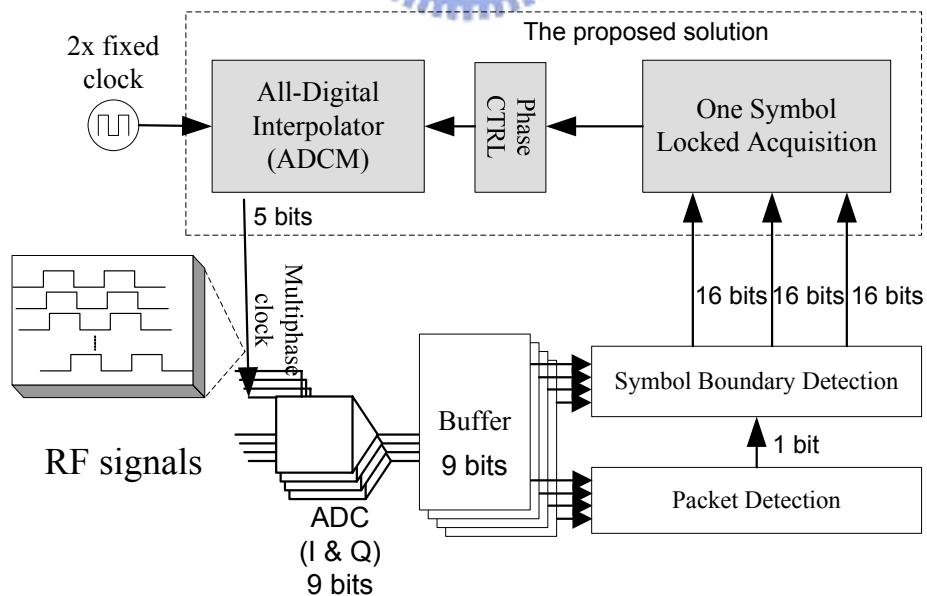
Figure 5-1: Data flow chart for hardware

5.1 Packet Synchronization

5.1.1 Packet Detection

Figure 5-2 illustrates the architecture of the packet detection. There are four sets calculators for each antenna to calculate u_i, as show in equation (3.5). One set calculator for geometric mean is used to come out u and the packet detection controller architecture was show in Figure 3-6.
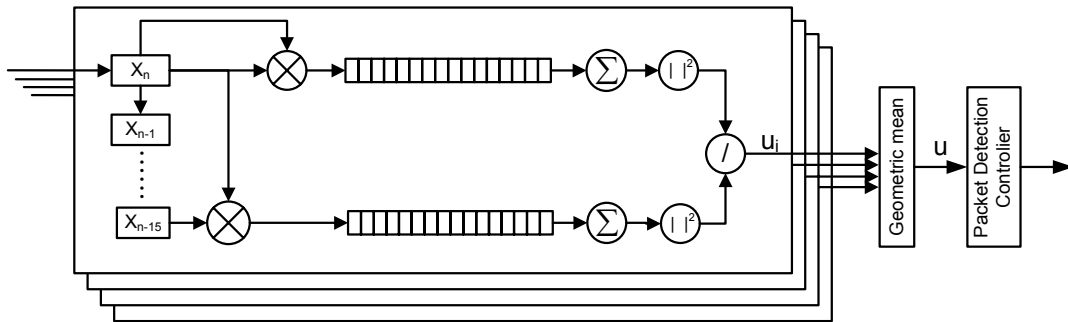
Figure 5-2: Hardware design of packet detection scheme

5.1.2 Symbol Boundary Detection

Figure 5-3 illustrates the architecture of the symbol boundary detection. There are four sets calculator for each antenna to calculate the boundary coefficients $P_{i,L}(k)$, and the definition of $Q_L(k)$ is show in equation (3.9). Then, $\hat{Symbol}_{index}$ Decision, which show in equation (3.11), generate a $\hat{Symbol}_{index}$ and pass boundary coefficient to timing synchronization.
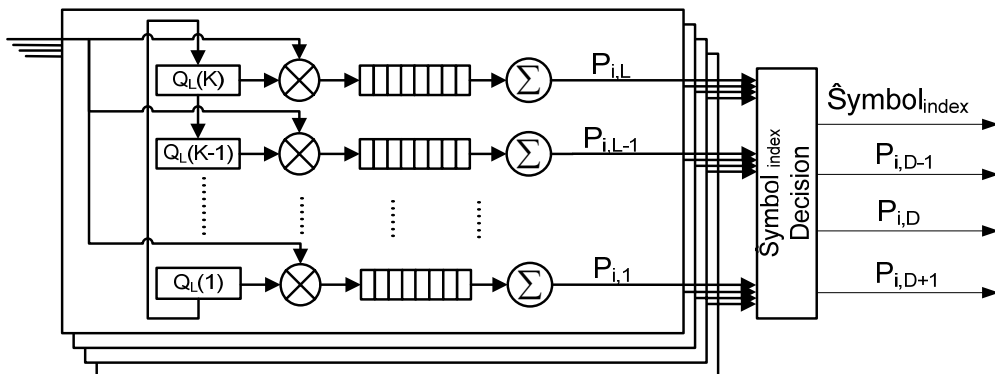
Figure 5-3: Hardware design of symbol boundary detection

5.2 Timing Synchronization

Figure 5-4 illustrates the architecture of the timing synchronization. There are four sets data buffer for each antenna, one packet detection and one symbol boundary detection. After received the three boundary coefficient from symbol boundary detection, the timing synchronization will locked the phase during one symbol by doing coarse and fine timing synchronization, the detail is show in section 3.2.
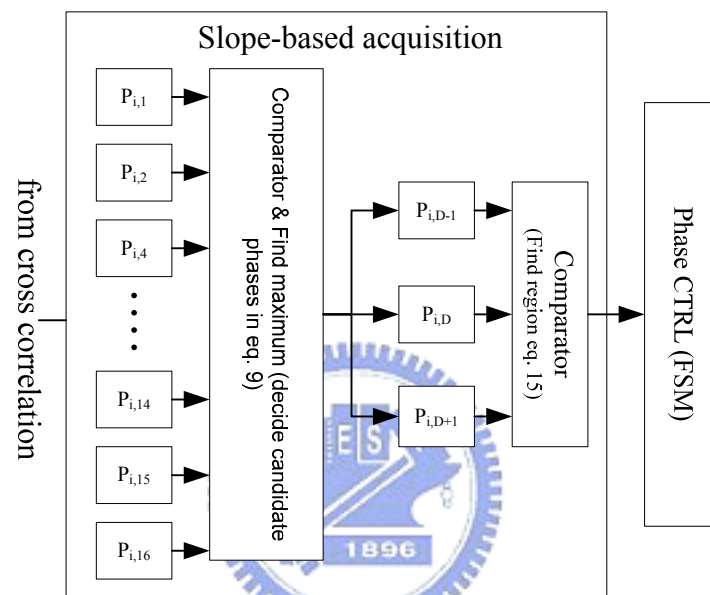
Figure 5-4: Hardware design of timing synchronization

5.3 Summary

Table 5-1 Hardware specifications

Hardware specifications	
Application	IEEE 802.11n MIMO-OFDM
Space-Time Coding	4×4 STBC
FFT/IFFT Size	64 point
Support Antenna Configuration	4 Tx, 1~4 Rx
Support Modulation Type	BPSK, QPSK, 16-QAM, 64-QAM
Technology	UMC 0.13 μm
System Clock	20 MHz

The hardware specifications, area report and power report are listed in Table 5-1, Table 5-2, and Table 5-3, respectively.

Table 5-2 Area report

Area Report	
Combinational area	919236.062500
Noncombinational area	235669.484375
Total cell area	1155449.000000

Table 5-3 Power report

Power Report	
Global Operating Voltage	1.08(V)
Cell Internal Power	10.3144 mW (82%)
Net Switching Power	2.2623 mW (18%)
Total Dynamic Power	12.5767 mW (100%)
Cell Leakage Power	1.0648 mW

Chapter 6

Conclusion and Future Work

I N this thesis, based on the share architecture and the preamble structure of IEEE 802.11n standard, a synchronization algorithm for IEEE 802.11n WLANs over TGN channels is proposed. A realistic channel model was employed, which includes the effects of physical channel, filtering, carrier offset, sampling clock offset, and impulsive inference. Loss in system performance due to synchronization error was used as a performance criterion.

6.1 Conclusion

In section 3.1.1, an autocorrelation based packet detection was introduced. The comparisons are shown in Table 6-1.

Table 6-1: Comparisons among state-of-the-art packet detection algorithm

	[16]	[17]	[18]	This work
Modulation	CPM	OFDM	OFDM	OFDM
Correlator	N/A	1	3	1
Detection method	One-shot	One-shot	One-shot	FSM
Correlation window	N/A	32 sample	32 sample	16 sample
Redetection period	3 symbols	N/A	N/A	1 symbol
Required SNR	10 dB	10 dB	2.5 dB	0 dB
Packet loss rate	10%	N/A	12%	<1%

In section 3.1.2, cyclic extension of L-STS is used to synchronize the symbol boundary. Since the estimator uses the inherent information of the OFDM preamble form the buffer, no additional training sequence is needed. The correlation window size B is set as 13 sample. The comparisons are shown in Table 6-2.

Table 6-2: Comparisons among state-of-the-art packet symbol boundary detection algorithm

	[22]	[24]	This work
System platform	OFDM	OFDM	OFDM
Hardware	Integration	Autocorrelation Moving-average	Crosscorrelation
Required Sample	16 sample	16/64 sample	13 sample
Required SNR	N/A	10 dB	5 dB

In section 3.2, a timing synchronization algorithm using the boundary coefficient to made decision was proposed. In other words, the timing synchronization shared the hardware architecture with symbol detection. A multiphase generator with 22 phases was used. Each of coarse and fine timing synchronization used half a L-STS, equal to 8 samples, the overall timing synchronization used a L-STS. The comparisons were shown in Table 6-3.

Table 6-3: Comparisons among state-of-the-art timing synchronization algorithm

	[25]	[26]	[27]	[28]	This work
System Type	Mixed-Mode	Mixed-Mode	All-Digital	All-Digital	All-Digital
Method	DAC + VCXO	DAC + VCXO	ADPLL (PTCG)	Non-PLL ADCM (Phase Interpolator)	Non-PLL ADCM (Phase Interpolator)
Control Factor	Freq.	Freq.	Phase (8 phases)	Phase (32 phases)	Phase (22 phases)
Over Sampling	N/A	4x	1x	1x	1x
Converge Cycle	40 symbols	380 symbols	N/A	4 symbols	1 symbols
Connect Structure	Off chip	Off chip	On chip	On chip	On chip

6.2 Future Work

A wireless communication system may experiment several kind of noise. In most of the cases, like thermal, atmospheric, or galactic noise, it can be represented by a Gaussian model. However, man-made noise that appears in urban environments cannot be assumed to be Gaussian. There are still some problems need to be solve. An exhaustive impulsive interference mode should be modified. Preamble and data compensations must be done.

As to the system, high QAM constellation likes 256-QAM for higher data rate is going to be deployed. Then, more antennas of transmitter and receiver like 8*8 are taken into consideration. Even huge FFT/IFFT (size bigger than 1000) is also a good research topic.

Bibliography

[1] T. Ojanperá and R. Prasad, "An overview of wireless broadband communications", *IEEE Commun. Mag.*, vol. 35, pp. 28-34, Jan. 1997.

[2] T. Pollet, M. Van Bladel, and M. Moeneclaey, "BER sensitivity of OFDM systems to carrier frequency offset and Wiener phase noise", *IEEE Trans. Commun.*, vol. 43, pp. 191-193, Feb./Mar./Apr. 1995 .

[3] M. Gudmundson and P.O. Anderson, "Adjacent channel interference in an OFDM system", in *Proc. Vehicular Technol. Conf.*, Atlanta, GA, May 1996, pp. 918-922.

[4] H. Minn, V. K. Bhargava, K. B. Letaief, "A robust timing and frequency synchronization for OFDM systems", *IEEE Trans. on wireless Commun.*, vol. 2, pp. 822-839, No. 4, July 2003.

[5] Hao Zhou, Malipatil A.V., Yih-Fang Huang, "Synchronization Issues in OFDM Systems", *Circuits and Systems, APCCAS 2006*, pp. 988-991, Dec 2006

[6] M. Speth, S. Fechtel, G. Fock, and H. Meyr, "Optimum Receiver Design for Wireless Broad-Band Systems Using OFDM – Part I", in *IEEE Trans. on Comm.*, vol. 47, no. 11, pp. 1668-1677, Nov.1999.

[7] 802.11n standard, "TGn Sync Proposal Technical Specification", IEEE 802.11-04/0889r7, July 2005.

[8] A. Palin, Symbol synchronization in DVB-T OFDM system, Master of Science Thesis, Tampere University of Technology, 1997.

[9] T. M. Schmidl, and D. C. Cox. "Robust Frequency and Timing Synchronization for OFDM-based WLANs", *IEEE Trans. Communications,* vol.45, No 12, pp. 1613-1621. Dec. 1997.

[10] P. Dent, G. Bottomley and T. Croft, "*Jakes Fading Model Revisited*", IEE Electronics Letters, p.1162~p.1163, June 1993

[11] W. C. Jakes, Ed., "*Microwave Mobile Communications*", IEEE Press, Piscataway, NJ, 1974

[12] J. Lago-Fernández. and. J. Salter J. Lago-Fernandez and J. Salter, "Modelling impulsive interference in DVB-T: statistical analysis, test waveforms & receiver performance", R&D white Paper, WHP080, April 2004.

[13] M.C. Jeruchim, P. Balaban, K.S. Shanmugan, *Simulation of Communication Systems: Modelling, Methodology, and Techniques*, 2nd Ed., Kluwer Academic / Plenum Publishers, Aug 2000.

[14] K. L. Blackard, T.S. Rappaport, and C.W. Bostian, "Measurements and Models of Radio Frequency Impulsive Noise for Indoor Wireless Communications", *IEEE Journal on Selected Areas in Comms.*, Vol. 11, No. 7, Sep 1993.

[15] IEEE P802.11 Wireless LANs, "Indoor MIMO WLAN Channel Models (Draft Document in Progerss_Rev1)", IEEE 802.11-03/161r1, July 11, 2003.

[16] Penrod R., Fitz M.P., Weijun Zhu, Takeshita O., "low complexity packet detection algorithm for a CPM modem" *Signals, Systems and Computers, 2004. Conference Record of the Thirty-Eighth Asilomar Conference on,* Vol. 1, pp. 1062-1067 Nov. 2004

[17] Ting-Jung Liang, Xin Li, Irmer R., Fettweis G., "Synchronization in OFDM-based WLAN with transmit and receive diversities" *Personal, Indoor and Mobile Radio Communications, 2005. PIMRC 2005. IEEE 16th International Symposium on,* Vol. 2, pp. 740-744, Sep 2005

[18] Ying Tan, Leyonhjem S., Faulkner M., "Timing Synchronization for OFDM-WLANs with Time Averaging Scheme", *Vehicular Technology Conference, 2006. VTC 2006-Spring. IEEE 63rd*, Vol. 4, pp. 1942-1946, 2006

[19] Chia-Hsiang Yang, Yu-Hsuan Lin, Shih-Chun Lin, Tzi-Dar Chiueh, "Design of a low-complexity receiver for impulse-radio ultra-wideband communication systems", *Circuits and Systems, 2004. ISCAS '04. Proceedings of the 2004 International Symposium on*, Vol. 4, pp.23-26, May 2004

[20] Calderbank A.R., Georghiades C.N., "Coding for the unsynchronized optical OPPM channel",*Communications, 1993. ICC 93. Geneva. Technical Program, Conference Record, IEEE International Conference on,* Vol. 1, pp.557-561, May 1993

[21] K. Witrisal, G. Leus, M. Pausini, and C. Krall, "Equivalent system model and equalization of differential impulse radio UWB systems," *IEEE J. Sel. Areas Commun.*, vol. 23, no. 9, pp. 1851-1862, Sept. 2005.

[22] Hsi-Chou Hsu, Jyh-Horng Wen, "Timing Synchronization in Ultra-Wideband Systems with Delay Line Combination Receivers", *Communications Letters, IEEE*, Vol. 11, pp. 264-266, March 2007

[23] Yi-Ju Chen, Yi-Ching Lei, Tzi-Dar Chiueh, "Baseband transceiver design for the DVB-terrestrial standard", *Circuits and Systems, 2004. Proceedings. The 2004*

IEEE Asia-Pacific Conference on, Vol. 1, pp.389-392, Dec. 2004

[24] Manusani S.K., Kshetrimayum R.S., Bhattacharjee R., "Robust Time and Frequency Synchronization in OFDM based 802.11a WLAN systems", *Annual India Conference, 2006*, pp. 1-4 , Sep. 2006

[25] J.Y. Yu, C.C. Chung, H.Y. Liu, and C.Y. Lee, "Power Reduction with Dynamic Sampling and All-Digital I/Q-Mismatch Calibration for A MB-OFDM UWB Baseband Transceiver," IEEE Symposium on VLSI Citcuits, June 2006.

[26] S. Sibecas, C.A. Emami, G. Stratis, and G. Rasor, "Pseudo-Pilot OFDM scheme for 802.11a and R/A in DSRC Applications," IEEE VTS-Fall, VTC, Oct 2003.

[27] A.I. Bo, G.E. Jian-hua, and W. Yong, "Symbol Synchronization Technique in COFDM Systems," IEEE Trans. Broadcasting, vol. 50, pp. 56-62, March 2004.

[28] Terng-Yin Hsu, You-Hsien Lin and Ming-Feng Shen, " Synchronous Sampling Recovery with All-Digital Clock Management in OFDM Systems", 2007